

Oxidation pathways and emission sources of atmospheric particulate nitrate in Seoul: based on δ15N and Δ17O measurements

Saehee Lim, Meehye Lee, Joel Savarino, Paolo Laj

▶ **To cite this version:**

Saehee Lim, Meehye Lee, Joel Savarino, Paolo Laj. Oxidation pathways and emission sources of atmospheric particulate nitrate in Seoul: based on δ15N and Δ17O measurements. Atmospheric Chemistry and Physics, 2022, 22, pp.5099-5115. 10.5194/acp-22-5099-2022 . insu-03706382

HAL Id: insu-03706382

https://insu.hal.science/insu-03706382

Submitted on 28 Jun 2022

HAL is a multi-disciplinary open access archive for the deposit and dissemination of scientific research documents, whether they are published or not. The documents may come from teaching and research institutions in France or abroad, or from public or private research centers.

L'archive ouverte pluridisciplinaire **HAL**, est destinée au dépôt et à la diffusion de documents scientifiques de niveau recherche, publiés ou non, émanant des établissements d'enseignement et de recherche français ou étrangers, des laboratoires publics ou privés.



Distributed under a Creative Commons Attribution 4.0 International License

Atmos. Chem. Phys., 22, 5099–5115, 2022
https://doi.org/10.5194/acp-22-5099-2022
© Author(s) 2022. This work is distributed under
the Creative Commons Attribution 4.0 License.

Atmospheric Chemistry and Physics
Open Access
EGU

Oxidation pathways and emission sources of atmospheric particulate nitrate in Seoul: based on $\delta^{15}N$ and $\Delta^{17}O$ measurements

Saehee Lim[1], Meehye Lee[1], Joel Savarino[2], and Paolo Laj[2]

[1]Department of Earth and Environmental Sciences, Korea University, Seoul 02841, South Korea
[2]Institute of Environmental Geosciences (IGE), Univ. Grenoble Alpes, CNRS, IRD, Grenoble INP, 38000 Grenoble, France

Correspondence: Meehye Lee (meehye@korea.ac.kr)

Received: 10 June 2021 – Discussion started: 19 July 2021
Revised: 4 January 2022 – Accepted: 25 January 2022 – Published: 19 April 2022

Abstract. $PM_{2.5}$ haze pollution driven by secondary inorganic NO_3^- has been a great concern in East Asia. It is, therefore, imperative to identify its sources and oxidation processes, for which nitrogen and oxygen stable isotopes are powerful tracers. Here, we determined the $\delta^{15}N$ (NO_3^-) and $\Delta^{17}O$ (NO_3^-) of $PM_{2.5}$ in Seoul during the summer of 2018 and the winter of 2018–2019 and estimated quantitatively the relative contribution of oxidation pathways for particulate NO_3^- and investigated major NO_x emission sources. In the range of $PM_{2.5}$ mass concentration from 7.5 $\mu g\,m^{-3}$ (summer) to 139.0 $\mu g\,m^{-3}$ (winter), the mean $\delta^{15}N$ was $-0.7‰ \pm 3.3‰$ and $3.8‰ \pm 3.7‰$, and the mean $\Delta^{17}O$ was $23.2‰ \pm 2.2‰$ and $27.7‰ \pm 2.2‰$ in the summer and winter, respectively. While OH oxidation was the dominant pathway for NO_3^- during the summer (87 %), nighttime formation via N_2O_5 and NO_3 was relatively more important (38 %) during the winter, when aerosol liquid water content (ALWC) and nitrogen oxidation ratio (NOR) were higher. Interestingly, the highest $\Delta^{17}O$ was coupled with the lowest $\delta^{15}N$ and highest NOR during the record-breaking winter $PM_{2.5}$ episodes, revealing the critical role of photochemical oxidation process in severe winter haze development. For NO_x sources, atmospheric $\delta^{15}N$ (NO_x) estimated from measured $\delta^{15}N$ (NO_3^-) considering isotope fractionation effects indicates vehicle emissions as the most important emission source of NO_x in Seoul. The contribution from biogenic soil and coal combustion was slightly increased in summer and winter, respectively. Our results built on a multiple-isotope approach provide the first explicit evidence for NO_3^- formation processes and major NO_x emission sources in the Seoul megacity and suggest an effective mitigation measure to improve $PM_{2.5}$ pollution.

1 Introduction

In northeast Asia, air pollution characterized by high $PM_{2.5}$ (particulate matter with aerodynamic diameter smaller than 2.5 µm) and ozone concentrations has received significant attention due to its serious effects on human health (Lelieveld et al., 2015; Xie et al., 2019). As a result of extensive efforts by East Asian countries to improve the ambient air quality, anthropogenic emissions of SO_x, NO_x, and CO have been significantly reduced, particularly in China (Cheng et al., 2019). Nonetheless, the number of severe haze events and the duration have been increased, which is not understood clearly.

It is also noteworthy that there are common chemical and meteorological characteristics in the occurrence of the $PM_{2.5}$ haze pollution in northeast Asia, such as inorganic-species-dominated chemical composition (Liu et al., 2018; Shao et al., 2018; Wang et al., 2019a) and transboundary transport of haze aerosol depending on the synoptic atmospheric circulation (Quan et al., 2020; Shi et al., 2020; Zheng et al., 2019). Overall, approximately 40 % of $PM_{2.5}$ consists of NO_3^-, SO_4^{2-}, and NH_4^+ (secondary inorganic aerosol, SIA) in both urban and background sites in China (Liu et al., 2018)

for the period of 2012–2013. The mass contribution of SIA was further augmented up to 69 % at urban Beijing and island sites (Changdao) in the North China Plain (NCP) during the 2016 spring (Lim et al., 2020). A large increase in SIA mass is particularly associated with efficient formation of NO_3^- in cold months (most frequently in December to March), leading to a rapid increase in $PM_{2.5}$ concentration and developing a persistent haze pollution on a regional scale (Li et al., 2018; Xu et al., 2019). Recent studies suggest that the regional occurrence of the $PM_{2.5}$ haze events derived by NO_3^- across the Asian continent has been associated with long-range transport of air pollutants promoted by cold fronts and their intrusion in downward regions by the development of the atmospheric boundary layer (Kang et al., 2019; Lee et al., 2019). However, scientific understanding is still limited because the rapid increase of fine-aerosol NO_3^- is the result of the complex interplay of oxidation and transformation mechanisms producing NO_3^- from various fossil and non-fossil sources of NO_x with micro-to-synoptic meteorology creating the conditions for NO_3^- formation. In addition, considering that NO_x emissions from bottom-up emission inventory are smaller than top-down estimates by satellites (e.g., Goldberg et al., 2019), our understanding of NO_x emissions is poor.

In order to better understand processes of NO_3^- formation including NO_x emission sources in East Asia, a growing number of recent studies have suggested nitrogen and oxygen stable-isotope-based measurement as a robust and useful tool for providing important clues for NO_3^- formation as well as NO_x emission sources (He et al., 2018; Lim et al., 2019, 2020; Song et al., 2019; Zong et al., 2017, 2020). The isotopic composition is expressed in parts per thousand (‰) and reported as δ (‰) $= (R_{\text{sample}}/R_{\text{standard}} - 1) \times 1000$ with R being the ratio of the heavy isotope over the light isotope (e.g., $^{15}N/^{14}N$, $^{18}O/^{16}O$, $^{17}O/^{16}O$) in a sample (R_{sample}) and in the international standard (R_{standard}). The international standards are the Vienna Standard Mean Ocean Water (VSMOW) and atmospheric N_2 for oxygen and nitrogen ratios. In terms of NO_x emission sources, the major NO_x sources are distinguished in their nitrogen isotopic compositions: biogenic soil (driven by fertilizer use; $-35.1‰ \pm 10.2‰$) (Felix and Elliott, 2014; Li and Wang, 2008; Yu and Elliott, 2017), biomass burning ($1.8‰ \pm 1.8‰$) (Fibiger and Hastings, 2016), vehicle emissions ($-2.5‰ \pm 1.5‰$) (Walters et al., 2015), and coal combustion ($14.2‰ \pm 4.5‰$) (Felix et al., 2012; Heaton, 1990). Despite evidence that $\delta^{15}N$ (NO_x) can serve as a useful tracer of NO_x emission sources, during NO_y photochemical cycling and its loss processes, the $\delta^{15}N$ of initial NO_x can be significantly altered by both kinetic and equilibrium isotopic fractionation effects (ε_N), complicating the link between $\delta^{15}N$ (NO_3^-) and $\delta^{15}N$ (NO_x) (Freyer et al., 1993; Li et al., 2020).

The formation processes of HNO_3 in the atmosphere consist of NO−NO_2 photochemical cycle Reactions (R1)–(R3) and post NO_2 oxidation Reactions (R4)–(R8). During the NO_x cycling, nitrogen isotopic fractionation is affected by unidirectional reactions of the Leighton cycle and NO_x isotope exchange equilibrium. A recent laboratory experiment has shown that the Leighton cycle isotope effect (LCIE) associated solely with O_3 Reaction (R1) and equilibrium isotopic effect (EIE) were $-10‰$ and $28.9‰$ at room temperature, respectively (Li et al., 2020). The relative importance of these two effects on $\delta^{15}N$ (NO_2) also depends on NO_x levels, leading to an increase (decrease) in $\delta^{15}N$ (NO_2) relative to $\delta^{15}N$ (NO_x) values at high (low) NO_x conditions (Kamezaki et al., 2019; Li et al., 2020; Walters et al., 2018). Overall, the nitrogen isotope exchange equilibrium has been suggested to be the dominant fractionation process in NO−NO_2 cycling at urban atmosphere (Freyer et al., 1993) and oxidation reactions forming nitric acid (HNO_3) and particulate NO_3^- (Savarino et al., 2013).

$$NO + O_3 \rightarrow NO_2 + O_2, \quad \text{(R1)}$$

$$NO + RO_2(HO_2) \rightarrow NO_2 + RO(OH), \quad \text{(R2)}$$

$$NO_2 + h\nu \rightarrow NO + O(^3P), \quad \text{(R3)}$$

$$NO_2 + OH \rightarrow HNO_3, \quad \text{(R4)}$$

$$NO_2 + O_3 \rightarrow NO_3 + O_2, \quad \text{(R5)}$$

$$NO_2 + NO_3 + \overset{M}{\longleftrightarrow} N_2O_5, \quad \text{(R6)}$$

$$N_2O_5 + H_2O \xrightarrow{aerosol} 2HNO_3(aq), \quad \text{(R7)}$$

$$NO_3 + RH \rightarrow HNO_3 + R, \quad \text{(R8)}$$

where M is an unreactive third body and R is any organic group.

The kinetic fractionation effect during daytime oxidation of NO_2 to HNO_3 Reaction (R4) is relatively minor, being estimated to be $-3‰$ (Freyer, 1991). During the nighttime when most NO is oxidized to NO_2 without NO_x photolysis, the isotopic equilibrium between NO_2, NO_3, and N_2O_5 should be achieved (Reaction R6). The nighttime thermal equilibrium likely favors the partitioning of ^{15}N into N_2O_5 relative to NO_2 and consequently induces a large isotopic fractionation effect of $25.5‰$ (Reactions R5–R6; Walters and Michalski, 2015). On the other hand, the nitrogen partitioning between NO_2 and NO_3 Reaction (R5) may induce a fractionation effect of about $-18‰$ (Walters and Michalski, 2015). These N isotope fractionation effects should be first evaluated to explore NO_x source contributions, which should be based on combining with a robust tracer for the contributions of NO_3^- oxidation pathways.

Lately, $\Delta^{17}O$ (NO_3^-) has been used for tracing NO_3^- oxidation pathways (Alexander et al., 2009, 2020; Morin et al., 2009; Savarino et al., 2007, 2013). Earlier researches observed that atmospheric NO_3^- is anomalously enriched in ^{17}O (Michalski et al., 2003), which stems from O_3 formation reactions, where a rare isotope effect leads to excess ^{17}O enrichment relative to what is expected based on the ^{18}O enrichments (Thiemens, 1999, 2006). This enrichment is quantified by $\Delta^{17}O$ notation (^{17}O excess, defined as $\delta^{17}O - 0.52 \times \delta^{18}O$). Since non-zero $\Delta^{17}O$ strictly reflects

a photochemical effect, NO_3^- produced by denitrification in soils should have $\Delta^{17}O$ of zero. The mass-independent $\Delta^{17}O$ signature of O_3 is transferred to NO_x, in which the number of oxygen atoms from O_3 is involved in NO_x. In this way, the $\Delta^{17}O$ (NO_3^-) is served as a conservative marker to track the chemical formation of atmospheric NO_3^-. Photochemical formation by peroxy radicals (HO_2 and RO_2) leads to a relatively low $\Delta^{17}O$ (NO_3^-), whereas nighttime formation through N_2O_5 and NO_3 results in high $\Delta^{17}O$ (Michalski et al., 2003; Morin et al., 2009; Savarino et al., 2007). Consequently, the difference in $\Delta^{17}O$ (NO_3^-) suggests approaching a proportional contribution of daytime and nighttime oxidation of NO_3^-.

To date, few field studies have coupled $\Delta^{17}O$ (NO_3^-) and $\delta^{15}N$ (NO_3^-) to investigate NO_x-to-NO_3^- oxidation processes and emission sources of NO_x, e.g., field researches in Japan (Nelson et al., 2018); West Virginia, USA (Rose et al., 2019); Shanghai, China (He et al., 2020); and Beijing, China (He et al., 2018; Song et al., 2020).

In this study, we present the measurement results of $\delta^{15}N$ and $\Delta^{17}O$ of NO_3^- in Seoul during the summer of 2018 and the winter of 2018–2019, when we encountered the record-breaking $PM_{2.5}$ concentrations. Then, the $\delta^{15}N$ and $\Delta^{17}O$ measurements are used to evaluate seasonally distinct atmospheric oxidation pathways of NO_3^- and to explore major NO_x source contributions in the study region.

2 Measurements and methods

2.1 Sampling

We collected $PM_{2.5}$ filter samples on the rooftop of the six-story Asan science building at the Korea University campus located in northeast Seoul, the capital of South Korea (37.59° N, 127.02° E; Fig. 1) during the summer of 2018 (26 May to 22 August; $n = 13$) and the winter of 2018–2019 (27 December to 8 March; $n = 18$). Seoul is a metropolitan area with a population of 9.77 million and known to be influenced by heavy road traffic all around. The $PM_{2.5}$ particulates were collected on quartz filters (20 cm × 25 cm; Pallflex Products, Putnam, USA) at a nominal flow rate of 96 m^3 hr^{-1} for 1 to 3 d using a high-volume air sampler (3000 series, Ecotech, Australia). Filters were analyzed for water-soluble ions, carbonaceous compounds, total nitrogen (TN) and carbon (TC), and stable nitrogen and oxygen isotopic ratios. Reactive gases including O_3, NO, NO_2, SO_2, and CO and a meteorological suite including air temperature, relative humidity, and wind speed and direction were measured hourly at the nearby monitoring sites run by the National Institute of Environmental Research (NIER) and the Korea Meteorological Administration (KAM), respectively. These data were averaged daily for comparison with filter-based chemical composition data, if necessary.

2.2 Chemical analyses

Filters were stored in a freezer pending chemical analysis. Chemical composition of $PM_{2.5}$ was determined for eight water-soluble ions (Cl^-, NO_3^-, SO_4^{2-}, Na^+, NH_4^+, K^+, Ca^{2+}, and Mg^{2+}) by ion chromatography (IC; Eco IC, Metrohm, Switzerland), organic carbon (OC) and elemental carbon (EC) by an OC-EC analyzer (Sunset Laboratory Inc., US) using the thermo-optical transmittance method (NIOSH870), and TC and total nitrogen (TN) by an elemental analyzer (EA, Fisons NA-1500NC, Thermo, Waltham, MA, USA). Mass concentrations of these constituents were corrected for laboratory and field blanks. The detection limit, determined as 3 standard deviations (SD) above blank concentrations, was <0.1 ppm for ionic species, 0.5 µg cm^{-3} for TC (the sum of OC and EC), and 0.8 g µgN and 0.5 µgC per punched filter area for TN and TC, respectively. Details of the analytical methods can be found elsewhere (Lim et al., 2020).

Following the bacterial denitrifier method (Casciotti et al., 2002; McIlvin and Casciotti, 2011), the $\Delta^{17}O$ of NO_3^- was measured simultaneously with $\delta^{18}O$ and $\delta^{15}N$ coupled with an isotope ratio mass spectrometry (IRMS) measurement using an in-house peripheral system at the Université Grenoble Alpes (Morin et al., 2009). In brief, NO_3^- of samples was converted to N_2O via bacterial denitrification, and the N_2O was further converted into O_2 and N_2, which were separated via a gas chromatography column before being introduced to the IRMS system (Thermo Finnigan MAT 253 isotope ratio mass spectrometer). Samples were measured in batch with reference materials following strictly the identical treatment principles, including the same water matrix for standards and samples. Together with samples, a subset of international nitrate reference materials (US Geological Survey 32, 34, and 35, as well as their mixtures) was measured for correction and calibration of $\Delta^{17}O$ and $\delta^{18}O$ values relative to VSMOW and $\delta^{15}N$ values relative to air N_2. The overall accuracy of the method is estimated as the reduced standard deviation of the residuals from the linear regression between the measured reference materials and their expected values (Morin et al., 2009). For these sets of analyses, the obtained uncertainties (1σ) were 0.4 ‰ and 0.3 ‰ for $\Delta^{17}O$ (NO_3^-) and $\delta^{15}N$ (NO_3^-), respectively. The analytical procedure used in this study strictly followed the method described in Morin et al. (2009), which adheres to the new standard bacterial method coupled with the gold catalyst for the thermal decomposition of N_2O into N_2 and O_2 (Kaiser et al., 2007).

2.3 Quantifying isotope fractionation effects

2.3.1 Isotope fractionation effects of NO_2 oxidation to atmospheric particulate NO_3^-: $\delta^{15}N$ (NO_3^-)

The HNO_3 forms through three major pathways including (i) OH pathway, (ii) O_3 pathway associated with N_2O_5, and (iii) O_3 pathway associated with NO_3.

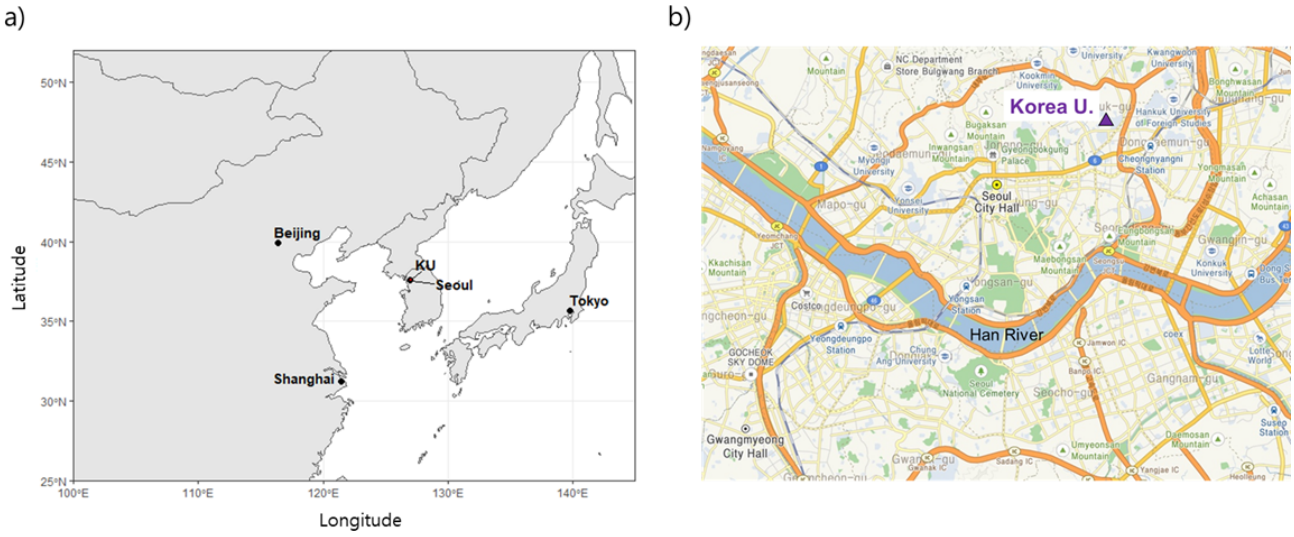


Figure 1. Location of the study region. **(a)** Seoul metropolitan area in South Korea; the map was generated using the open-source software R (http://www.R-project.org/, last access: 2 February 2021). **(b)** Sampling site of the Korea University campus in the northeast Seoul; the map was taken from © Kakao maps (https://map.kakao.com/, last access: 29 December 2021).

OH pathway

When NO and NO_2 coexist in similar quantities due to the Leighton cycle, ^{15}N is preferentially partitioned into NO_2 via the equilibrium isotope effect, leading to higher $\delta^{15}N$ in NO_2 relative to NO and NO_x (Freyer et al., 1993; Walters et al., 2016). Considering the comparable concentrations of NO and NO_2 over a year in Seoul (Fig. S1 in the Supplement), the N isotope effects on $\delta^{15}N$ (NO_3^-) should be significantly affected by NO_x photochemical interactions. The relative importance of EIE and LCIE to $\delta^{15}N(NO_2)$ can be assessed by comparing lifetimes of NO_2 with respect to isotope exchange with NO ($\tau_{exchange}$) and photolysis (τ_{NO_2+hv}). In this regard, the "A" factor was defined as $\tau_{exchange}/\tau_{NO_2+hv} = j_{NO_2}/k_1 \times [NO] (k_1 = 8.14 \times 10^{-14}\,cm^3\,s^{-1}$, Sharma et al., 1970) by Li et al. (2020, 2021). These studies demonstrated that A was as small as 0.01–0.5 in the EIE-dominated regime with NO_x >20 ppbv and the ratio of NO_2/NO_x <0.6. In Seoul, to simply evaluate the relative importance of EIE and LCIE only (not for ^{15}N correction), the A factor was estimated to be 0.08 ± 0.20 (median $\pm$ SD) and 0.60 ± 0.51 during the winter and summer months, respectively, indicating the significant influence of the equilibrium isotope effect on $NO-NO_2$ isotopic fractionation. The time series j_{NO_2} was calculated using the Master Chemical Mechanism (MCM) model (Saunders et al., 2003).

After NO_x photochemical cycling, NO_2 is oxidized by the reaction with OH radical to form atmospheric HNO_3 (HNO_3 Reaction R4 pathway). The N fractionation effect of particulate NO_3^- produced via the HNO_3 Reaction (R4) pathway (ε_1, unit in ‰) can be expressed as the following, neglecting kinetic isotope effects associated with the HNO_3 Reaction (R4) pathway (Walters and Michalski, 2016):

$$\delta^{15}N(HNO_3)(R4) = \delta^{15}N(NO_2) = \delta^{15}N(NO_x) + \varepsilon_1, \quad (1a)$$

$$\varepsilon_1 = \left(\left({}^{15}\alpha_{NO_2/NO} - 1\right)\left(1 - f_{NO_2}\right)\right) / \left(\left(1 - f_{NO_2}\right) + \left({}^{15}\alpha_{NO_2/NO} \times f_{NO_2}\right)\right), \quad (1b)$$

where f_{NO_2} is the fraction of NO_2 relative to the total NO_x, and ${}^{15}\alpha_{NO_2/NO}$ is the temperature-dependent isotope equilibrium exchange fractionation factor for NO_2/NO (Walters et al., 2016). In the present study, the measured f_{NO_2} was used individually for summer samples, and a seasonal mean f_{NO_2} (0.69) was applied to winter samples due to the lack of availability of continuous $NO-NO_2$ measurement data.

Oxidation of NO_x to HNO_3 is regarded as the formation pathway of particulate NO_3^- via the HNO_3 Reaction (R4) pathway due to the unconstrained isotope fractionation effect between HNO_3 and NO_3^-, resulting in the following equation:

$$\delta^{15}N(HNO_3)\ (R4) = \delta^{15}N\left(NO_3^-\right)(R4). \quad (1c)$$

O_3 pathways associated with N_2O_5 and NO_3

During the nighttime when NO is oxidized into NO_2 without photolyzing back to NO and fresh emissions of NO are negligible, NO_x exists almost as NO_2, and thus $\delta^{15}N$ (NO_2) should be reflective of the $\delta^{15}N$ of NO_x sources. If NO_2 is oxidized to N_2O_5, the isotopic equilibrium is likely to be achieved between NO_2, NO_3, and N_2O_5 by chemical equilibrium Reaction (R6), and the $\delta^{15}N$ values of N_2O_5 and NO_3 will reflect the isotope equilibrium fractionation factors relative to NO_2 (i.e., ${}^{15}\alpha_{N_2O_5/NO_2}$ and ${}^{15}\alpha_{NO_3/NO_2}$; values were adopted from the Supplement Table S5 in Walters

and Michalski, 2016). Finally, δ^{15}N of particulate NO_3^- produced from dark pathways can be expressed as the following, neglecting currently unconstrained kinetic isotopic fractionation associated with Reactions (R7) and (R8) (Walters and Michalski, 2016):

$$\delta^{15}\mathrm{N}(\mathrm{HNO_3})(\mathrm{R7}) = \delta^{15}\mathrm{N}(\mathrm{N_2O_5}) = \delta^{15}\mathrm{N}(\mathrm{NO_2}) + \varepsilon_2, \quad (2a)$$

$$\varepsilon_2 = \left({}^{15}\alpha_{\mathrm{N_2O_5/NO_2}-1}\right), \quad (2b)$$

$$\delta^{15}\mathrm{N}(\mathrm{HNO_3})(\mathrm{R7}) = \delta^{15}\mathrm{N}\left(\mathrm{NO_3^-}\right)(\mathrm{R7}), \quad (2c)$$

$$\delta^{15}\mathrm{N}(\mathrm{HNO_3})(\mathrm{R8}) = \delta^{15}\mathrm{N}(\mathrm{NO_3}) = \delta^{15}\mathrm{N}(\mathrm{NO_2}) + \varepsilon_3, \quad (3a)$$

$$\varepsilon_3 = \left({}^{15}\alpha_{\mathrm{NO_3/NO_2}-1}\right), \quad (3b)$$

$$\delta^{15}\mathrm{N}(\mathrm{HNO_3})(\mathrm{R8}) = \delta^{15}\mathrm{N}\left(\mathrm{NO_3^-}\right)(\mathrm{R8}). \quad (3c)$$

Therefore, the δ^{15}N (NO_x) in the atmosphere can be expressed using measured δ^{15}N (NO_3^-) and the net N isotope fractionation effect, ε_N.

$$\delta^{15}\mathrm{N}(\mathrm{NO}_x)_{\mathrm{atmosphere}} = \delta^{15}\mathrm{N}\left(\mathrm{NO_3^-}\right)_{\mathrm{measured}} - \varepsilon_\mathrm{N}, \quad (4a)$$

$$\varepsilon_\mathrm{N} = \varepsilon_1 \times f_1 + \varepsilon_2 \times f_2 + \varepsilon_3 \times f_3, \quad (4b)$$

where ε_1, ε_2, and ε_3 are the abovementioned N isotope fractionation effect of pathways (i), (ii), and (iii), respectively, and the proportional contributions (f_1, f_2, and f_3) of the three NO_3^- formation pathways were estimated from Δ^{17}O measurements (Sect. 2.3.2).

2.3.2 Proportional contributions of three formation pathways to atmospheric particulate NO_3^- : Δ^{17}O (NO_3^-)

Due to its mass-independent nature, Δ^{17}O of particulate NO_3^- is a conservative tracer of photochemical NO_3^- formation (Michalski et al., 2003, 2004). At photochemical steady state, the Δ^{17}O of NO_2 is determined by the relative production rate of NO_2 via O_3 oxidation Reaction (R1) in NO_2 production Reactions (R1) and (R2) (f_{O_3}) and the mass-independent Δ^{17}O anomaly transferred from O_3 during Reaction (R1) ($\Delta^{17}\mathrm{O}{-}\mathrm{O}_3^*$):

$$\Delta^{17}\mathrm{O}(\mathrm{NO_2})(‰) = f_{\mathrm{O_3}} \times \Delta^{17}\mathrm{O}{-}\mathrm{O}_3^*. \quad (5)$$

f_{O_3} was adopted from a previous study conducted in Beijing (Wang et al., 2019b), where the seasonal mean was 0.858 and 0.918 for summer and winter, respectively. $\Delta^{17}\mathrm{O}{-}\mathrm{O}_3^*$ can be approximated as $1.5 \times \Delta^{17}\mathrm{O}{-}\mathrm{O_3}$ because of the isotopic asymmetry of O_3 (Michalski and Bhattacharya, 2009). In this study, the $\Delta^{17}\mathrm{O}{-}\mathrm{O}_3^*$ is $37.5‰ \pm 2.2‰$ (mean $\pm$ SD) averaged from literature sources as the isotopic composition of ozone shows a remarkable stability in the lower troposphere (Ishino et al., 2017; Vicars et al., 2012; Vicars and Savarino, 2014)

The Δ^{17}O of particulate NO_3^- produced via the three formation pathways can be predicted by distinct Δ^{17}O transfer functions as the following (Morin et al., 2011):

$$\begin{aligned}\Delta^{17}\mathrm{O}\left(\mathrm{NO_3^-}\right)(\mathrm{R4})(‰) &= 2/3\Delta^{17}\mathrm{O}(\mathrm{NO_2}) \\ &= 2/3\, f_{\mathrm{O_3}} \times \Delta^{17}\mathrm{O}{-}\mathrm{O}_3^*, \end{aligned} \quad (6a)$$

$$\begin{aligned}\Delta^{17}\mathrm{O}\left(\mathrm{NO_3^-}\right)(\mathrm{R7})(‰) &= 5/6\Delta^{17}\mathrm{O}(\mathrm{N_2O_5}) \\ &= 1/3\Delta^{17}\mathrm{O}(\mathrm{NO_2}) + 1/2\Delta^{17}\mathrm{O}(\mathrm{NO_3}) \\ &= 1/6\Delta^{17}\mathrm{O} - \mathrm{O}_3^*\left(4 f_{\mathrm{O_3}} + 1\right), \end{aligned} \quad (6b)$$

$$\begin{aligned}\Delta^{17}\mathrm{O}\left(\mathrm{NO_3^-}\right)(\mathrm{R8})(‰) &= \Delta^{17}\mathrm{O}(\mathrm{NO_3}) \\ &= 2/3\Delta^{17}\mathrm{O}(\mathrm{NO_2}) + 1/3\Delta^{17}\mathrm{O}{-}\mathrm{O}_3^* \\ &= 1/3\Delta^{17}\mathrm{O}{-}\mathrm{O}_3^*\left(2 f_{\mathrm{O_3}} + 1\right). \end{aligned} \quad (6c)$$

Finally, the Δ^{17}O (NO_3^-) can be expressed as the following:

$$\begin{aligned}\Delta^{17}\mathrm{O}\left(\mathrm{NO_3^-}\right)_{\mathrm{measured}} &= \Delta^{17}\mathrm{O}\left(\mathrm{NO_3^-}\right)(\mathrm{R4}) \times f_1 \\ &+ \Delta^{17}\mathrm{O}\left(\mathrm{NO_3^-}\right)(\mathrm{R7}) \times f_2 \\ &+ \Delta^{17}\mathrm{O}\left(\mathrm{NO_3^-}\right)(\mathrm{R8}) \times f_3, \end{aligned} \quad (7)$$

where Δ^{17}O (NO_3^-)$_{measured}$ is the measured value in this study, and the three endmember values of Δ^{17}O (NO_3^-) Reaction (R4), Δ^{17}O (NO_3^-) Reaction (R7), and Δ^{17}O (NO_3^-) Reaction (R8) are calculated using Eqs. (6a)–(6c). The proportional contributions of the three NO_3^- formation pathways ($f_1 + f_2 + f_3 = 1$) were estimated by the Stable Isotope Analysis in R (SIAR) model (Sect. 2.5) for the winter and the summer months.

2.4 Estimation of $PM_{2.5}$ aerosol liquid water content (ALWC) and aerosol pH

ISORROPIA II is a thermodynamic equilibrium model for the Cl^-, NO_3^-, SO_4^{2-}, Na^+, NH_4^+, K^+, Ca^{2+}, Mg^{2+}, and H_2O aerosol system (Fountoukis and Nenes, 2007). In the present study, the model was run as a forward and metastable mode to calculate aerosol liquid water content (ALWC) and pH. The detailed information of the model is found in Fountoukis and Nenes (2007). As input parameters, the concentrations of water-soluble ions that were measured by NIER and ambient RH and temperature were used for the model.

2.5 Bayesian stable isotope mixing model (stable isotope analysis in R, SIAR)

For quantifying proportional contribution of three NO_3^- formation pathways (f_1, f_2, and f_3 in Eq. 4b), we used the Bayesian stable isotope mixing model (Parnell et al., 2013) implemented in the simmr package in R software, which is available at https://cran.r-project.org/web/packages/simmr/

index.html (last access: 10 March 2021). The Bayesian Markov chain Monte Carlo approach is adequate to provide the relative contribution of the endmembers. Detailed information of the SIAR can be found in Parnell et al. (2010). As input data, measured $\Delta^{17}O$ (NO_3^-) and estimated $\Delta^{17}O$ (NO_3^-) endmember values of each pathway were treated in the SIAR model. Similar use of the SIAR model can be found elsewhere (Song et al., 2020; Wang et al., 2019b).

2.6 Backward air mass trajectory

Two-day air mass backward trajectories were analyzed using the HYSPLIT (Hybrid Single-Particle Lagrangian Integrated Trajectory) model with meteorological input from the global data assimilation system (a regular $1° \times 1°$ longitude–latitude grid) (Stein et al., 2015; https://ready.arl.noaa.gov/HYSPLIT.php, last access: 27 May 2020). The trajectories were calculated every 6 h at an elevation of 500 m a.s.l. The potential source contribution function (PSCF) was then applied to calculate the probable source location (latitude i and longitude j), which is determined here as the ratio of the number of trajectory end points associated with measured $\delta^{15}N$ (NO_3^-) values higher than a threshold value (set to the 95th percentile of $\delta^{15}N$ (NO_3^-) (m_{ij}) to the total number of points (n_{ij}) in the ijth grid cell). The PSCF calculation and the determination of the gridded trajectory frequencies were made in the openair R package (https://cran.r-project.org/web/packages/openair/index.html, last access: 4 January 2021) (Carslaw and Ropkins, 2012).

3 Results and discussion

3.1 Seasonal characteristics of $PM_{2.5}$ concentration, $\delta^{15}N$ (NO_3^-), and $\Delta^{17}O$ (NO_3^-)

$PM_{2.5}$ mass concentration varied from 7.5 to 139.0 $\mu g\,m^{-3}$ for the whole sampling period. According to the typical synoptic weather patterns of East Asia (Kim et al., 2007), the measurements are divided into summer (May–August) and winter (October–March) groups. A clear seasonal difference in $PM_{2.5}$ concentration and its composition were observed with significantly higher concentrations of mass and inorganic constituent in the winter than in the summer (Table 1 and Fig. S1).

During the summer, $PM_{2.5}$ concentration ranged from 7.5 to 34.5 $\mu g\,m^{-3}$ with a mean of $22.7 \pm 6.9\,\mu g\,m^{-3}$. The mean concentration of TC and TN was $4.6 \pm 1.4\,\mu gC\,m^{-3}$ and $1.9 \pm 1.0\,\mu gN\,m^{-3}$, respectively, resulting in the mean TC / TN ratio of 2.7 ± 2.0. The mass concentrations of all measured species were much higher in the winter, during which $PM_{2.5}$ concentration was raised up to 139.0 from 10.6 $\mu g\,m^{-3}$ with a mean of $61.7 \pm 39.2\,\mu g\,m^{-3}$. Accordingly, the mean of TC and TN was $15.2 \pm 4.5\,\mu gC\,m^{-3}$ and $11.8 \pm 7.7\,\mu gN\,m^{-3}$, respectively, and the mean TC / TN ratio of 0.9 ± 0.7 was noticeably lower than that of the summer.

For the entire experiment, the mean mass fraction against $PM_{2.5}$ was the highest for NO_3^- ($26\,\% \pm 23\,\%$), followed by SO_4^{2-} ($20\,\% \pm 1\,\%$) and NH_4^+ ($14\,\% \pm 1\,\%$), highlighting the contribution of SIA to $PM_{2.5}$ mass. The NO_3^- mass concentration varied from 0.2 to 69.3 $\mu g\,m^{-3}$ with a mean of $17.6 \pm 22.1\,\mu g\,m^{-3}$. Seasonally, the NO_3^- concentration was significantly higher in the winter ($29.7 \pm 22.1\,\mu g\,m^{-3}$) than summer ($0.8 \pm 0.9\,\mu g\,m^{-3}$). TN existed completely as inorganic N from both NO_3^- and NH_4^+ during the winter (regression slope of 1.0). During the summer, NO_3^- and NH_4^+ comprised 67 % of TN, and the rest (33 %) was assumed to be organic nitrogen (ON) components. In contrast, the mass fraction of SO_4^{2-} against $PM_{2.5}$ was higher in the summer (23 %) than winter (19 %). The seasonal characteristics of chemical composition imply the significant role of inorganic nitrogen species in $PM_{2.5}$ mass increase in winter and ON and sulfate in summer.

Both $\delta^{15}N$ (NO_3^-) and $\Delta^{17}O$ (NO_3^-) exhibited an inverse correlation with ambient temperature ($r = -0.87$ and $r = -0.55$, respectively). The $\delta^{15}N$ (NO_3^-) exhibited higher values in winter with a weight mean of $-0.7\,‰ \pm 3.3\,‰$ and $3.8\,‰ \pm 3.7\,‰$ in the summer and the winter, respectively. This seasonal pattern of $\delta^{15}N$ (NO_3^-) has been typically observed in East Asia regions (Li et al., 2019; Song et al., 2019; Zong et al., 2020). Analysis of backward air mass trajectory indicates that the lower and the upper bound of $\delta^{15}N$ (NO_3^-) were associated with air masses from the ocean by southerly and easterly winds in the summer and from Siberia by northerly winds in winter, respectively (Fig. S3 in the Supplement). In comparison with urban China (Fig. 2a), averaged summer $\delta^{15}N$ (NO_3^-) values were comparable between Seoul and all urban Chinese sites reported here, whereas in winter, $\delta^{15}N$ (NO_3^-) of Seoul was similar to that of Shanghai and Guangzhou rather than $\delta^{15}N$ (NO_3^-) of Beijing, which was higher than 10 ‰. Another observation at a mountain station in Taiwan shows that the highest $\delta^{15}N$ (NO_3^-) was found in spring when the level of anthropogenic constituents was elevated (Guha et al., 2017). These observations over East Asia may suggest to some extent that the seasonal pattern of $\delta^{15}N$ (NO_3^-) is basically associated with a synoptic meteorological condition that controls the type and strength of emission sources, where low and high $\delta^{15}N$ (NO_3^-) values indicate biogenic soil emissions and fossil combustion, respectively (Elliott et al., 2019).

Along with nitrogen isotope, heavier oxygen isotopes were also enriched in NO_3^- during the winter compared to the summer, when the weight-mean values of $\delta^{17}O$, $\delta^{18}O$, and $\Delta^{17}O$ in NO_3^- were $70.4\,‰ \pm 5.4\,‰$, $82.0\,‰ \pm 6.2\,‰$, and $27.7\,‰ \pm 2.2\,‰$ for the winter and $57.3\,‰ \pm 4.9\,‰$, $65.7\,‰ \pm 6.2\,‰$, and $23.2\,‰ \pm 2.2\,‰$ for the summer. These results of high winter and low summer $\Delta^{17}O$ (NO_3^-) were consistent with previous observations at urban Beijing (He et al., 2018; Wang et al., 2019b; Fig. 2b), indicative of relatively greater contribution of nighttime oxidation pathways

Table 1. Measurement summary of $PM_{2.5}$ chemical constituents and isotopic compositions in Seoul during the sampling period of May 2018–March 2019. Arithmetic mean ± 1 SD (mass fraction, %) for mass concentrations and concentration-weighted mean ± 1 SD for isotope ratios.

Constituents	Summer ($n = 13$)	Winter ($n = 18$)
$PM_{2.5}$ ($\mu g\,m^{-3}$)	22.7 ± 6.9	61.7 ± 39.2
TC	4.6 ± 1.4 (20 %)	15.2 ± 4.5 (25 %)
TN	1.9 ± 1.0 (8 %)	11.8 ± 7.7 (19 %)
NO_3^-	0.8 ± 0.9 (4 %)	29.7 ± 22.1 (48 %)
NH_4^+	1.9 ± 0.8 (8 %)	11.7 ± 8.4 (19 %)
SO_4^{2-}	5.3 ± 2.1 (23 %)	11.5 ± 9.2 (19 %)
$[NH_4^+]$ / ($[SO_4^{2-}]+[NO_3^-]$) equiv. ratio	0.83 ± 0.08	0.94 ± 0.09
$\delta^{15}N$ (NO_3^-)	−0.7 ± 3.3	3.8 ± 3.7
$\delta^{17}O$	57.3 ± 4.9	70.4 ± 5.4
$\delta^{18}O$	65.7 ± 6.2	82.0 ± 6.2
$\Delta^{17}O$	23.2 ± 2.2	27.7 ± 2.2

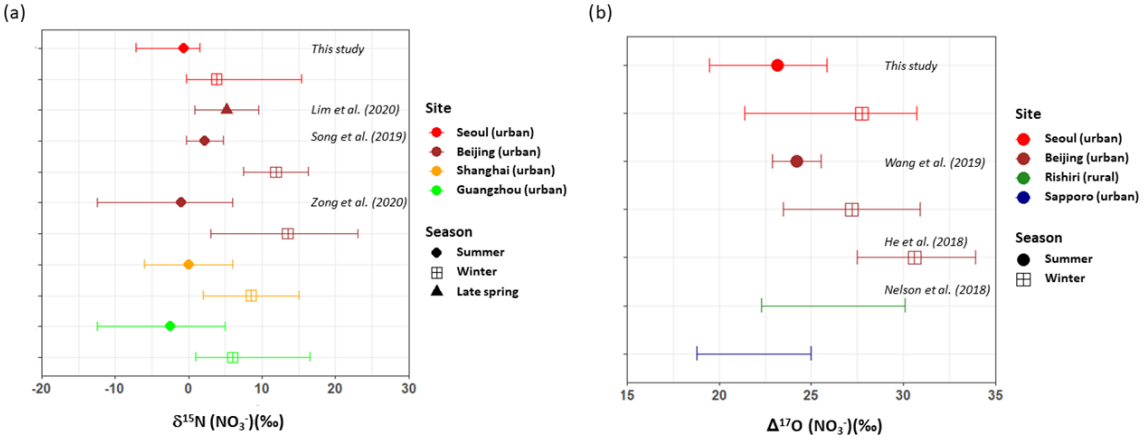


Figure 2. **(a)** $\delta^{15}N$ (NO_3^-) and **(b)** $\Delta^{17}O$ (NO_3^-) $PM_{2.5}$ observed in northeast Asia are compared: Seoul in this study (red); Beijing (brown), Shanghai (orange), and Guangzhou (light) in China; and Rishiri (green) and Sapporo (blue) in Japan during summer (circle) and winter (square). Annual ranges were presented for Rishiri and Sapporo. Marker indicates mean value (concentration-weighted average for Seoul samples of the present study), and lower and upper whiskers denote minimum and maximum values (this study; He et al., 2018; Lim et al., 2020; Nelson et al., 2018), mean ± SD (Song et al., 2019; Wang et al., 2019b), or 25th and 75th percentiles (Zong et al., 2020). Different marker shapes indicate different seasons.

in winter. It is also noteworthy that our summer and winter $\Delta^{17}O$ (NO_3^-) values were similar to annual $\Delta^{17}O$ (NO_3^-) values of an urban (Sapporo) and a rural (Rishiri) site in Japan, respectively (Nelson et al., 2018). It is likely suggestive that the winter $\Delta^{17}O$ value in Seoul has undergone a considerable atmospheric processing on a regional scale.

Given that $PM_{2.5}$ concentrations reflect the seasonality, atmospheric chemical composition and meteorological properties were examined in relation to $PM_{2.5}$ concentrations (Fig. 3). Clearly, for the winter samples with $PM_{2.5}$ concentration greater than 40 $\mu g\,m^{-3}$, meteorological conditions varied relative to low $PM_{2.5}$ samples; relatively high temperature and RH staying at 0 to 10° and 45 % to 65 %, respectively, and a low wind speed of 1 to 2 $m\,s^{-1}$, representing the meteorological characteristics of winter $PM_{2.5}$ episodes. Particularly in winter, a strong linearity of $PM_{2.5}$ was found with most chemical constituents considered in this study, such as SIA species, TN, NOR, and SOR (sulfur oxidation ratio). However, although elevated in level, NO_2 and O_3 mixing ratios showed non-linearity with $PM_{2.5}$ concentrations. Isotope ratios were correlated either linearly or inversely with $PM_{2.5}$ concentrations. In winter, $\Delta^{17}O$ (NO_3^-) showed the best correlation with $PM_{2.5}$ concentrations, but $\delta^{15}N$ (NO_3^-) was inversely related with $PM_{2.5}$ level.

3.2 Graphical representation of dual isotopes: $\Delta^{17}O$ and $\delta^{15}N$ of NO_3^-

The isotope ratios of source endmembers are scarce in the study region and in the aerosol measurements, and the iso-

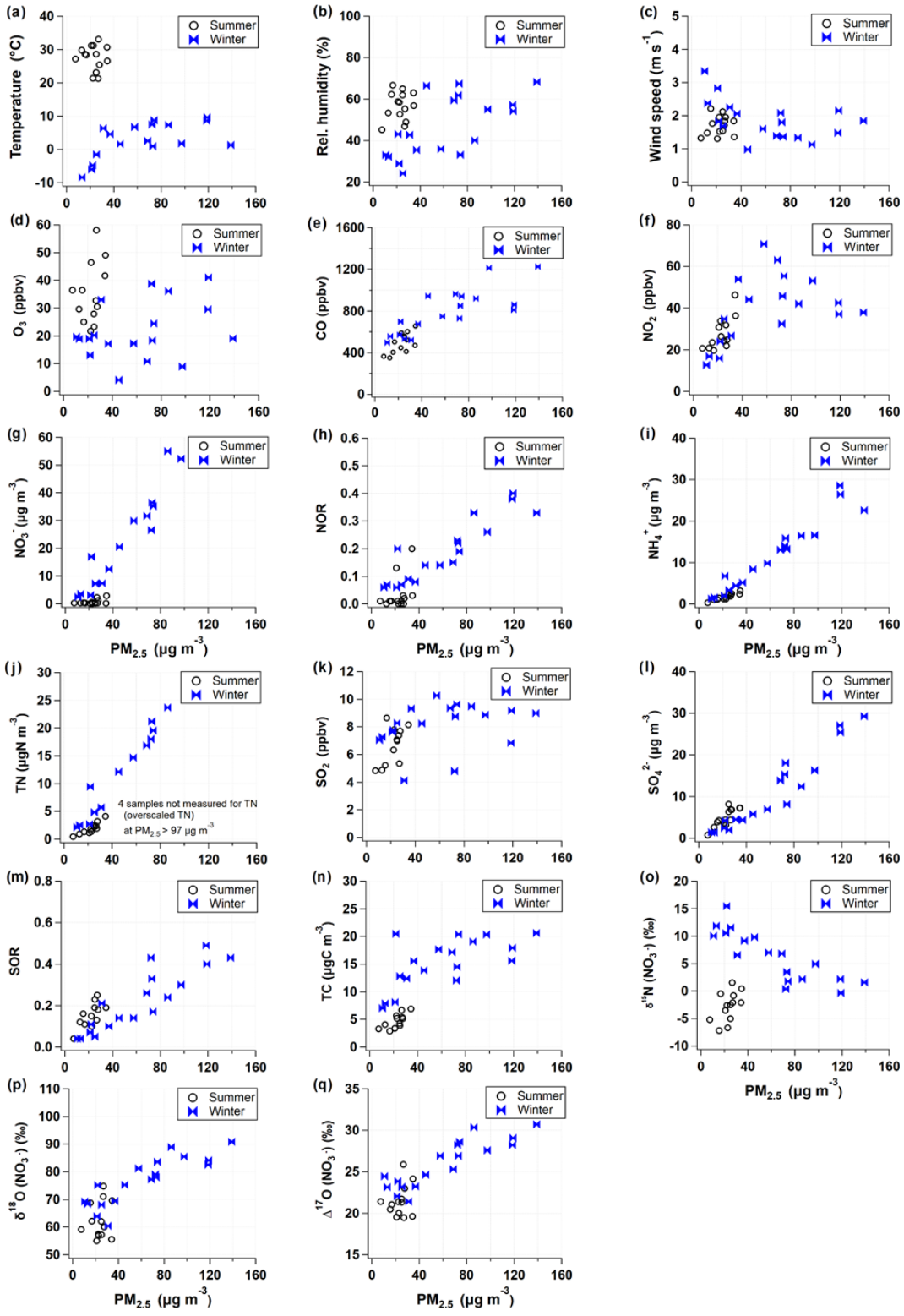


Figure 3. Relationships of $PM_{2.5}$ mass concentration with meteorological parameters **(a–c)**, concentrations of reactive gases **(d–f, k)** and aerosol chemical constituents **(g–j, l–n)**, and N and O isotopic compositions **(o–q)** measured in Seoul during the summer (open circle) and the winter (blue ribbon).

tope fractionation effect during gas-to-particle conversion is often estimated with thermodynamic constants and reasonable assumptions. In this regard, the graphical representation of dual isotopes enables the complex signatures of atmospheric samples to be distinguished and allows their oxidation processes to be constrained. Figure 4 displays measured $\delta^{15}N$ (NO_3^-) and $\Delta^{17}O$ (NO_3^-) coordinates with related chemical parameters in colors.

In Fig. 4a and b, the range of $\Delta^{17}O$ (NO_3^-) endmembers for the three NO_3^- oxidation pathways calculated in Sect. 2.3.2 is presented by black dotted boxes, which are successfully distinguished. The $\Delta^{17}O$ (NO_3^-) values of all samples fell into the predicted ranges of the $\Delta^{17}O$ endmembers but were separated into seasonal groups. Most of summer $\Delta^{17}O$ (NO_3^-) values indicate the NO_3^- Reaction (R4) pathway. It is in accordance with what has been reported in temperate areas during summer (Alexander et al., 2009; Michalski et al., 2003). In field measurements of $\delta^{15}N$ (NO_3^-) and $\delta^{18}O$ (NO_3^-) in Chinese cities, the proportional contribution of the OH-oxidation pathway was significantly correlated with latitudes (Zong et al., 2020), confirming the evidence of the NO_3^- formation through OH oxidation depending on UV radiation intensity.

In comparison, more than half of winter samples are located in the domains indicating NO_3^- Reactions (R7) and (R8) pathways. In particular, for winter samples with NO_3^- mass concentration higher than $\sim 30\,\mu g\,m^{-3}$, $\Delta^{17}O$ (NO_3^-) values clearly represent the Reaction (R7) pathway. The winter $\Delta^{17}O$ (NO_3^-) was proportional to the NOR (Fig. 4c), which is indicative of the efficient conversion of NO_x to NO_3^- via O_3 oxidation pathways. In the summer periods when NO_3^- concentrations were relatively high (above $\sim 3\,\mu g\,m^{-3}$), the contributions of O_3 oxidation pathways became elevated, which is a similar pattern to what was observed in the winter. This result suggests that the O_3 oxidation pathways are likely to be responsible for the rapid conversion of particulate NO_3^- observed during winter and summer $PM_{2.5}$ episodes in the study region.

The formation of N_2O_5 Reaction (R6) is dependent on both NO_2 and O_3, which are reciprocally correlated in source regions. The equilibrium of Reaction (R6) shifts to N_2O_5 at low temperature, and its lifetime against photolysis is long under the low sunlight. For these reasons, the dark formation of NO_3^- Reaction (R7) would be favorable in urban outflows in winter. The hydrolysis of N_2O_5 on aerosol surface Reaction (R7) is highly dependent on RH, aerosol liquid water content (ALWC), and chemical composition (Hallquist et al., 2003; Wahner et al., 1998). To evaluate the $\Delta^{17}O$ (NO_3^-) signature observed, we calculated ALWC and acidity of aerosol, pH, using the ISORROPIA II model (Sect. 2.4). Given the high concentration of nano-particles from various sources in the urban areas, it is assured that aerosol surface is enough for the NO_3^- Reaction (R7) pathway. The calculated ALWC was higher by 90 % ($19.1 \pm 22.8\,\mu g\,m^{-3}$) in the winter and lower by 21 % ($7.8 \pm 5.2\,\mu g\,m^{-3}$) in the summer relative to the annual mean of the 2 years. When NO_3^- mass concentrations were greater than $\sim 3\,\mu g\,m^{-3}$ in the summer and $\sim 30\,\mu g\,m^{-3}$ in the winter, ALWC was 14.3 and $31.7\,\mu g\,m^{-3}$, respectively, which were greater by 166 % and 183 % than the seasonal mean, respectively (Fig. 4d). Furthermore, the high $\Delta^{17}O$ (NO_3^-) and ALWC coincided with the lower bound (about 4) of winter pH varying from 4 to 6, whereas aerosol pH was 2–3 during the summer. The low aerosol pH concurrent with the high $\Delta^{17}O$ (NO_3^-) and ALWC is coherent with the aqueous-phase HNO_3 formation on liquid aerosol through Reaction (R7).

While $\Delta^{17}O$ (NO_3^-) allows insights into the oxidation pathway of NO_3^-, $\delta^{15}N$ (NO_3^-) values are affected by various factors, most of which are not well constrained due to the complicated chemistry of nitrogen oxides in the Earth's environment. In this study, $\delta^{15}N$ (NO_3^-) variability versus $PM_{2.5}$ concentration resembled the variability of NO_2 versus $PM_{2.5}$ concentration (Fig. 3f and o), implying a close link between NO_2 oxidation and $\delta^{15}N$ (NO_3^-). Therefore, in addition to the role of $\Delta^{17}O$ (NO_3^-) as a tracer of an NO_3^- oxidation pathway, we evaluated whether a variation of $\delta^{15}N$ (NO_3^-) indicates NO_x oxidation efficiency between NO and NO_2 (Freyer et al., 1993; Nelson et al., 2018; Walters et al., 2016). A possible effect on $\delta^{15}N$ during NO_x photochemical cycling cannot be predicted in the same way under varying conditions of NO, NO_2, and O_3 abundances. The shift in $\delta^{15}N$ (NO_2) relative to $\delta^{15}N$ (NO_x) in the atmosphere will change depending on f_{NO_2} and temperature-dependent $\alpha_{NO_2/NO}$ (Freyer et al., 1993; Li et al., 2020; Walters et al., 2016). When O_3 mixing ratio is high, NO is almost completely oxidized to NO_2, leading to an increasing f_{NO_2} value, and the $\delta^{15}N$ (NO_2) should correspond to the $\delta^{15}N$ of NO_x sources (Freyer et al., 1993).

In the dual isotope coordinates of $\delta^{15}N$ (NO_3^-) and $\Delta^{17}O$ (NO_3^-) (Fig. 4), it is evident that the samples taken during a record-breaking winter's $PM_{2.5}$ pollution events are associated with the lower bound values of $\delta^{15}N$ (NO_3^-) (−1 ‰ to 4 ‰) and the highest $\Delta^{17}O$ (NO_3^-) values (28 ‰ to 31 ‰). Simultaneous measurements of PM_1 chemical composition in Seoul and Beijing demonstrated that the regionally processed air masses were long-range transported to Seoul within approximately 2 d during these episodes (H. Kim et al., 2020). Their NO_2/O_3 ratio (1 to 2) was clearly lower with higher f_{NO_2} (0.7 to 0.8) compared to the other winter samples (Fig. 4g and h). This result implies that O_3 level was high enough to efficiently oxidize NO to NO_2 during the severe $PM_{2.5}$ pollution events. In this condition, the shift in $\delta^{15}N$ (NO_2) relative to $\delta^{15}N$ (NO_x) is insignificant, and, consequently, $\delta^{15}N$ (NO_2) would be lower than those of other winter samples unless both emission sources and $\alpha_{NO_2/NO}$ changed significantly. Considering that NO_3^- is the key driver of the high $PM_{2.5}$ in Seoul, the higher degree of NO_x oxidation efficiency is worth highlighting, in conjunction with a strong linear relationship between $\Delta^{17}O$ (NO_3^-) and NOR (Fig. 4c) revealing an efficient

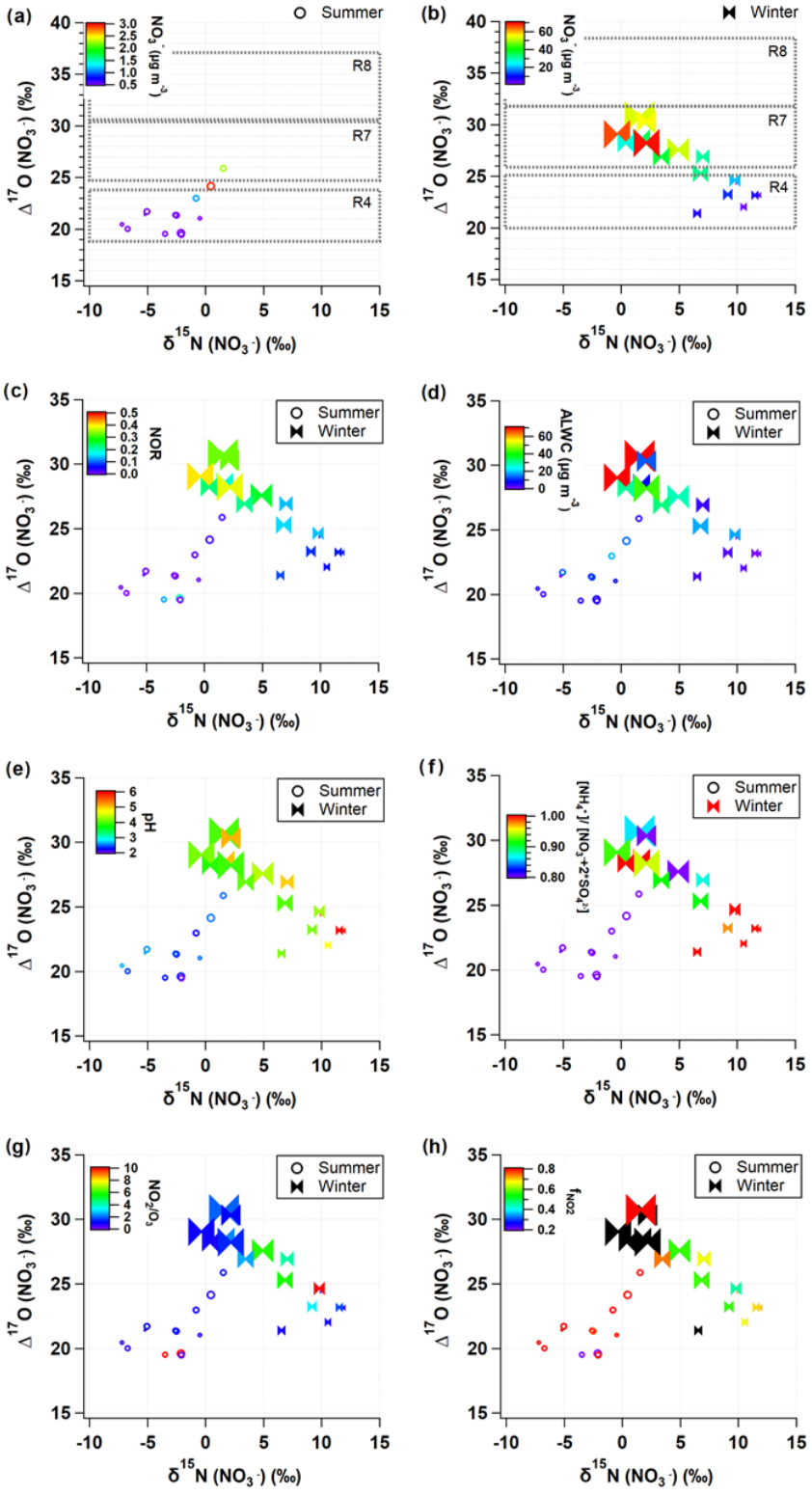


Figure 4. Relationship of measured $\delta^{15}N$ (NO_3^-) and $\Delta^{17}O$ (NO_3^-) values with key parameters during the summer (open circle) and winter (closed ribbon). The predicted $\Delta^{17}O$ (NO_3^-) values are presented as dotted rectangles for the three major NO_3^- formation pathways (Reactions R4, R7, and R8; see Sect. 2.3.2 for details) in **(a)** summer and **(b)** winter. Data are color coded by **(a, b)** nitrate concentrations, **(c)** NOR, **(d)** ALWC, **(e)** pH, **(f)** $[NH_4^+]/([SO_4^{2-}] + [NO_3^-])$ equivalent ratio, **(g)** NO_2/O_3 ratio, and **(h)** f_{NO_2}. Marker size is proportional to $PM_{2.5}$ concentration ranging from 10 to 100 $\mu g\,m^{-3}$.

conversion of NO_2 to NO_3^- through NO_3^- pathway Reactions (R5)+(R6)+(R7)+(R8) via O_3.

3.3 Contributions of major HNO_3 oxidation pathways

Combining the $\Delta^{17}O$ (NO_3^-) measurements and the calculation of $\Delta^{17}O$ transferred from O_3 to HNO_3, the contributions of three major NO_3^- formation pathways were quantitatively accounted for, despite the inherent uncertainties in the calculation (Sect. 2.5).

NO_3^- pathway Reaction (R4) dominated the total NO_3^- formation ($87\,\% \pm 6\,\%$) in summer. In contrast, the nighttime pathways through N_2O_5 and NO_3 (pathways Reactions R7 and R8) were responsible for 24 % and 14 % of the NO_3^- formation in the winter, respectively. The contributions increased further to 40 % and 30 %, respectively, on haze days when $PM_{2.5}$ concentration exceeded $75\,\mu g\,m^{-3}$, the "very bad" alert of the national air quality standard. The significant nighttime oxidation of NO_3^- has been observed broadly at urban sites in northeast Asia. The results of this study are consistent with those conducted in Beijing, showing low $\Delta^{17}O$ values in summertime (about 17 ‰ to 25 ‰) and substantially high $\Delta^{17}O$ values (about 25 ‰ to 34 ‰) in wintertime when NO_3^--driven $PM_{2.5}$ haze pollution occurred (He et al., 2018; Song et al., 2020; Wang et al., 2019b). In general, nighttime pathways accounted for more than 60 % and up to 97 % in Beijing (He et al., 2018; Song et al., 2020; Wang et al., 2019b). From a global perspective, the chemical transport model demonstrated that N_2O_5 heterogeneous hydrolysis was of comparable importance to $NO_2 + OH$ (41 %) for NO_3^- formation at below 1 km altitude (Alexander et al., 2020).

It is noteworthy that although the seasonal patterns are similar in northeast Asia, the average proportional contributions estimated from $\Delta^{17}O$ (NO_3^-) are highly sensitive to input parameters (i.e, f_{O_3} and $\Delta^{17}O{-}O_3^*$). In this study, the seasonal f_{O_3} was assumed to be equal to those estimated for Beijing and set to 0.858 ± 0.05 and 0.918 ± 0.05 for the warm and cold months, respectively (Wang et al., 2019b), which are comparable to other estimates for Beijing (0.86) and Shanghai (0.97) (He et al., 2018, 2020) and the annual mean of 0.85 in a global model (Alexander et al., 2020).

The uncertainty associated with $\Delta^{17}O{-}O_3^*$ has been recognized as the largest source of uncertainty in estimating NO_3^- production pathways from $\Delta^{17}O$ (NO_3^-) (Alexander et al., 2009, 2020). In this study, the $\Delta^{17}O{-}O_3^*$ of $37.5\,‰ \pm 2.2\,‰$ was averaged from previous observations, corresponding to $\Delta^{17}O$-bulk O_3 of 25 ‰ (Ishino et al., 2017; Vicars et al., 2012; Vicars and Savarino, 2014). Our mean $\Delta^{17}O{-}O_3^*$ of 37.5 ‰ was 2.8 ‰ higher and 1.5 ‰ lower than what was used in the field studies (Song et al., 2020; Wang et al., 2019b) and other studies (He et al., 2018, 2020), respectively, for urban Beijing and Shanghai. When a sensitivity test was conducted for the proportional contribution of the three oxidation pathways, a 2.8 ‰ change in $\Delta^{17}O{-}O_3^*$ value caused a 1.6 ‰, 2.1 ‰, and 2.5 ‰ change in the endmember for the pathways for Reactions (R4), (R7), and (R8), respectively. As a result, the average contribution of the nighttime pathways, including NO_3^- Reaction (R7) and NO_3^- Reaction (R8), increased to 23 % in summer and 65 % in winter. This suggests that a proper use of key parameters driving endmember values is a prerequisite for more realistic quantification of NO_3^- oxidation pathway contributions.

3.4 Major NO_x emission sources

To investigate major emission sources of atmospheric NO_x in Seoul, $\delta^{15}N$ (NO_x) in the atmosphere ($\delta^{15}N$ $(NO_x)_{atmosphere}$) was estimated from measured $\delta^{15}N$ (NO_3^-) considering nitrogen isotopic fractionation effects (ε_N) based on a dual isotopes approach ($\Delta^{17}O$ and $\delta^{15}N$). Estimated ε_N values were $5.9\,‰ \pm 1.5\,‰$ and $12.2\,‰ \pm 0.5\,‰$, and accordingly the $\delta^{15}N$ $(NO_x)_{atmosphere}$ was $-8.7\,‰ \pm 3.3\,‰$ and $-5.8\,‰ \pm 4.2\,‰$ in summer and winter, respectively. The larger winter ε_N reveals the enhanced contribution of the nighttime oxidation pathway via N_2O_5. As a result, a seasonal difference in $\delta^{15}N$ $(NO_x)_{atmosphere}$ was as small as 2.9 ‰ on average, which is suggestive of little seasonal difference in major NO_x emission sources in Seoul.

Figure 5 displays the measured $\delta^{15}N$ (NO_3^-) and estimated $\delta^{15}N$ $(NO_x)_{atmosphere}$ of individual samples together with $\delta^{15}N$ (NO_x) domains of emission source endmembers reported in literature: biogenic soil (driven by fertilizer use, $-35.1\,‰ \pm 10.2\,‰$; Felix and Elliott, 2014; Li and Wang, 2008; Yu and Elliott, 2017), biomass burning ($1.8\,‰ \pm 1.8\,‰$; Fibiger and Hastings, 2016), vehicle emissions ($-2.5\,‰ \pm 1.5\,‰$; Walters et al., 2015), and coal combustion ($14.2\,‰ \pm 4.5\,‰$; Felix et al., 2012; Heaton, 1990). Both in summer and winter, $\delta^{15}N$ $(NO_x)_{atmosphere}$ values are the closest to the domain of vehicle emissions $\delta^{15}N$ (NO_x), highlighting the largest contribution of vehicle emissions to NO_x in Seoul (Fig. 5). However, the winter $\delta^{15}N$ (NO_3^-) without isotope fractionation effect apparently points to coal emissions, which could lead to misleading conclusions about major NO_x sources. This result is supported by a better correlation of NO_2 with CO than with SO_2 for both seasons. According to an (anthropogenic) bottom-up emissions inventory, the Clean Air Policy Support System (CAPSS), total mobile sources account for about two-thirds of NO_x emissions in Korea, followed by combustion sources such as energy and manufacturing industries (33 %). The highest NO_2 column densities are distinct in Seoul metropolitan areas, which is mostly due to the emissions from transportation (H. C. Kim et al., 2020). Our results of the isotope measurements are in fairly good agreement with the national emission inventories and satellite observations, highlighting the largest contribution of vehicle emissions to NO_x sources in Seoul.

Other than vehicle emissions, the lower bound summer $\delta^{15}N$ $(NO_x)_{atmosphere}$ and the upper bound win-

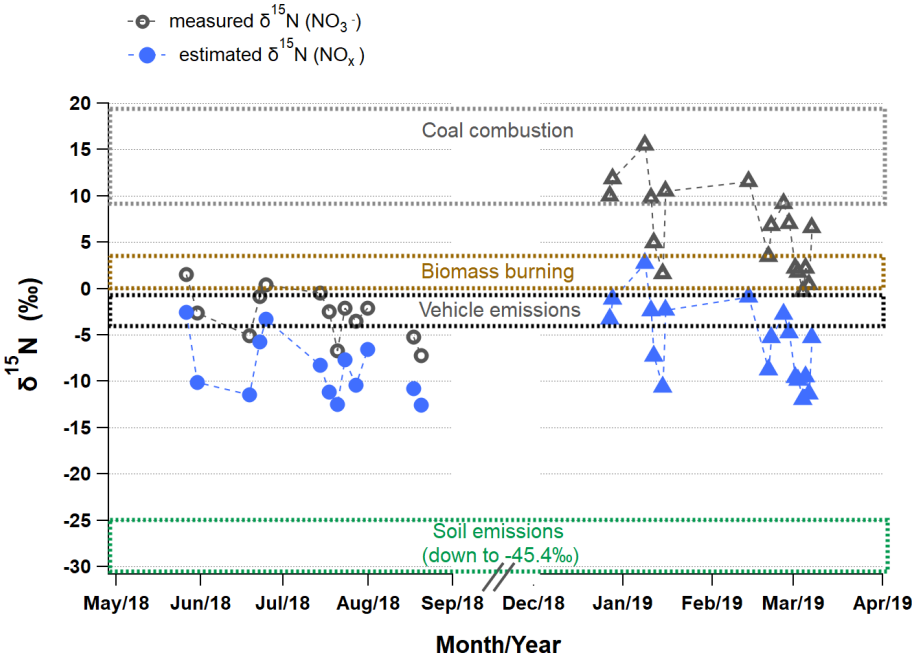


Figure 5. Variations in measured δ^{15}N (NO_3^-) (open) and estimated δ^{15}N $(NO_x)_{atmosphere}$ (closed) in Seoul during the summer (circle) and winter (triangle). The δ^{15}N (NO_x) range (mean ± 1 SD) of source endmembers is distinguished by dotted boxes in different colors: coal combustion (14.2 ‰±4.5 ‰; Felix et al., 2012; Heaton, 1990), biomass burning (1.8 ‰ ± 1.8 ‰; Fibiger and Hastings, 2016), vehicle emissions (−2.5 ‰ ± 1.5 ‰; Walters et al., 2015), and biogenic soil emissions (−35.1 ‰ ± 10.2 ‰; Felix and Elliott, 2014; Li and Wang, 2008; Yu and Elliott, 2017).

ter δ^{15}N $(NO_x)_{atmosphere}$ were relatively closer to the δ^{15}N (NO_x) of fertilized soil emissions and coal combustion, respectively. These seasonally distinct contributions from soil emissions and coal combustion were consistent with the results from previous studies conducted in China, revealing common seasonal emission characteristics on a regional scale in East Asia. It was evident that the upper bound winter δ^{15}N $(NO_x)_{atmosphere}$ coincided with an elevated SO_4^{2-}/NO_3^- mass ratio by 2–3 times. During these periods, trajectory analysis indicates that air masses originated from cold regions in northeastern China, such as Liaoning province, where heavy and coal-fired industries are located. In Beijing, located in northeastern China, coal combustion is an important fossil-fuel source as the highest contribution source to atmospheric NO_x emissions during winter, about 30 % to 40 %, regardless of approaches used for estimating NO_3^- oxidation pathways, either Δ^{17}O or δ^{18}O (Li et al., 2019; Song et al., 2019, 2020; Zong et al., 2020). Thus, in this study, the upper bound winter δ^{15}N $(NO_x)_{atmosphere}$ suggests enhanced contributions of coal combustion to atmospheric NO_x emissions. It is particularly noteworthy that the lower winter δ^{15}N (NO_3^-) and thus relatively lower contribution of coal combustion of the present study confirms the recent trend that emissions from coal combustion have been reduced in China (Cheng et al., 2019; Tong et al., 2018). Our study was conducted in later years (2018–2019) than their studies (2013–2017), in which δ^{15}N (NO_3^-) values were rather comparable to the winter mean δ^{15}N (NO_3^-) observed in Seoul during January 2014 to February 2016 (11.9 ‰ ± 2.5 ‰; Park et al., 2018). The lower bound of winter δ^{15}N (NO_3^-) values associated with the highest NO_3^- and $PM_{2.5}$ concentrations (Figs. 3 and 4) was considered a result of complex effects of isotopic fractionation, as discussed above.

This study region is under the influence of various biomass burning sources throughout a year, such as agricultural combustion in the vicinities of Seoul and over eastern China from spring to fall (Chen et al., 2017; Zhao et al., 2017), wild fires over Siberia and the Russian Far East in summer (van der Werf et al., 2010), and residential biomass combustion for heating over east Asia in winter. Some winter δ^{15}N $(NO_x)_{atmosphere}$ values fell in the δ^{15}N (NO_x) range of biomass burning endmembers (Fibiger and Hastings, 2016; Fig. 5). When assessing contributions of biomass burning based on few endmember δ^{15}N (NO_x), however, caution should be exerted considering the fact that δ^{15}N (NO_x) varied among biomass types from −7 ‰ to 12 ‰ (Fibiger and Hastings, 2016), and there is currently a lack of understanding of biomass combustion that could potentially affect air quality in Seoul.

4 Conclusions and outlook

Our δ^{15}N- and Δ^{17}O-based study confirms that vehicle emissions are the main source of NO_3^- in $PM_{2.5}$ in Seoul during the summer and the winter. In addition, the qualitative estimates of NO_x emission sources provide suggestive evidence for enhanced contributions from coal combustion and biogenic soil emissions in the winter and the summer, respectively. Moreover, severe winter haze events with daily $PM_{2.5}$ exceeding $100\,\mu g\,m^{-3}$ were mainly driven by NO_3^- (up to $\sim 60\,\%$ in $PM_{2.5}$). Reducing NO_x emissions from vehicles is, therefore, essential for an effective mitigation measure to improve fine aerosol pollution in the study region. In particular, the highest $PM_{2.5}$ was concurrent with the lowest $\delta^{15}N$ (NO_3^-) and the highest $\Delta^{17}O$ (NO_3^-) and NOR, revealing the efficient NO-to-NO_2 conversion and heterogeneous conversion of HNO_3 to particulate NO_3^- through the O_3 oxidation pathway during the winter haze episodes. The multiple-isotope signatures of particulate NO_3^-, including ^{17}O, ^{18}O, and ^{15}N, highlight the secondary nature of fine aerosol pollution intimately coupled with the photochemical oxidation process.

While our results demonstrate that $\delta^{15}N$ and $\Delta^{17}O$ are robust tracers for major NO_x sources, quantitative source apportionment using the isotope method requires further elaboration of isotope equilibrium and/or kinetic fractionation effects involved in photochemical cycling of nitrogen oxides and $\delta^{15}N$ of NO_x source endmembers representing local or regional emissions in East Asia. In well-designed field studies, the $\delta^{15}N$ and $\Delta^{17}O$ measurements of multiphase and their vertical structures allow us to test the isotope fractionation effects suggested by laboratory experiments and theoretical calculations, as well as to characterize the atmospheric processing that influences them. In addition, there is an urgent need to document the $\delta^{15}N$ (NO_x) values of emissions from vehicles with/without selective catalytic reduction (SCR) and from biomass combustion as a function of biomass type and combustion conditions. Consequently, a comprehensive and quantitative understanding of the oxidation pathways and emission sources of nitrogen oxides using $\delta^{15}N$ and $\Delta^{17}O$ measurements will be able to elucidate the detailed mechanisms driving severe haze development in megacities of northeast Asia, including Seoul.

Data availability. Data used in this study are available upon request to the corresponding author.

Supplement. The supplement related to this article is available online at: https://doi.org/10.5194/acp-22-5099-2022-supplement.

Author contributions. SL and ML conceived the project and carried out the aerosol sampling and the analysis of aerosol chemical compositions. SL conceptualized and wrote the article. ML supervised the study and wrote the article. JS conducted stable isotope analysis on the samples and helped SL in interpreting the results. The results of the study were discussed by all authors but especially by PL.

Competing interests. The contact author has declared that neither they nor their co-authors have any competing interests.

Disclaimer. Publisher's note: Copernicus Publications remains neutral with regard to jurisdictional claims in published maps and institutional affiliations.

Special issue statement. This article is part of the special issue "Effect of Megacities on the Transport and Transformation of Pollutants at Regional and Global Scales (EMeRGe) (ACP/AMT interjournal SI)". It is not associated with a conference.

Acknowledgements. This research was supported by the National Strategic Project Fine Particle of the National Research Foundation of Korea (NRF), funded by the Ministry of Science and ICT (MSIT), Ministry of Environment (ME), and Ministry of Health and Welfare (MOHW) (grant no. 2017M3D8A1092015). Funding to Saehee Lim was provided by the National Research Foundation of Korea (NRF) from the Ministry of Science and ICT (grant no. 2018R1D1A1B07050849). Meehye Lee thanks for the support from NRF (grant no. 2020R1A2C3014592). Joel Savarino thanks the French National Research Agency (Investissements d'avenir grant no. ANR-15-IDEX-02) and the INSU program LEFE-CHAT for supporting the stable isotope laboratory. This is publication 4 of PANDA platform on which isotope analyses were performed. The authors especially thank Nicolas Caillon for performing the analysis of the ammonium–nitrogen isotope ratio. The authors thank the Korea National Institute of Environmental Research (NIER) and Korea Meteorological Administration (KMA) for their monitoring data used in this study.

Financial support. This research has been supported by the National Research Foundation of Korea (grant nos. 2017M3D8A1092015, 2018R1D1A1B07050849, and 2020R1A2C3014592).

Review statement. This paper was edited by Manabu Shiraiwa and reviewed by two anonymous referees.

References

Alexander, B., Hastings, M. G., Allman, D. J., Dachs, J., Thornton, J. A., and Kunasek, S. A.: Quantifying atmospheric nitrate formation pathways based on a global model of the oxygen isotopic composition ($\Delta^{17}O$) of atmospheric nitrate, Atmos. Chem.

Phys., 9, 5043–5056, https://doi.org/10.5194/acp-9-5043-2009, 2009.

Alexander, B., Sherwen, T., Holmes, C. D., Fisher, J. A., Chen, Q., Evans, M. J., and Kasibhatla, P.: Global inorganic nitrate production mechanisms: comparison of a global model with nitrate isotope observations, Atmos. Chem. Phys., 20, 3859–3877, https://doi.org/10.5194/acp-20-3859-2020, 2020.

Carslaw, D. C. and Ropkins, K.: openair – An R package for air quality data analysis, Environ. Model. Softw., 27–28, 52–61, https://doi.org/10.1016/j.envsoft.2011.09.008, 2012.

Casciotti, K. L., Sigman, D. M., Hastings, M. G., Bohlke, J. K., and Hilkert, A.: Measurement of the oxygen isotopic composition of nitrate in seawater and freshwater using the denitrifier method, Anal. Chem., 74, 4905–4912, https://doi.org/10.1021/ac020113w, 2002.

Chen, J., Li, C., Ristovski, Z., Milic, A., Gu, Y., Islam, M. S., Wang, S., Hao, J., Zhang, H., He, C., Guo, H., Fu, H., Miljevic, B., Morawska, L., Thai, P., LAM, Y. F., Pereira, G., Ding, A., Huang, X., and Dumka, U. C.: A review of biomass burning: Emissions and impacts on air quality, health and climate in China, Sci. Total Environ., 579, 1000–1034, https://doi.org/10.1016/j.scitotenv.2016.11.025, 2017.

Cheng, J., Su, J., Cui, T., Li, X., Dong, X., Sun, F., Yang, Y., Tong, D., Zheng, Y., Li, Y., Li, J., Zhang, Q., and He, K.: Dominant role of emission reduction in $PM_{2.5}$ air quality improvement in Beijing during 2013–2017: a model-based decomposition analysis, Atmos. Chem. Phys., 19, 6125–6146, https://doi.org/10.5194/acp-19-6125-2019, 2019

Elliott, E. M., Yu, Z., Cole, A. S., and Coughlin, J. G.: Isotopic advances in understanding reactive nitrogen deposition and atmospheric processing, Sci. Total Environ., 662, 393–403, https://doi.org/10.1016/J.SCITOTENV.2018.12.177, 2019.

Felix, J. D. and Elliott, E. M.: Isotopic composition of passively collected nitrogen dioxide emissions: Vehicle, soil and livestock source signatures, Atmos. Environ., 92, 359–366, https://doi.org/10.1016/j.atmosenv.2014.04.005, 2014.

Felix, J. D., Elliott, E. M., and Shaw, S. L.: Nitrogen Isotopic Composition of Coal-Fired Power Plant NO_x: Influence of Emission Controls and Implications for Global Emission Inventories, Environ. Sci. Technol., 46, 3528–3535, https://doi.org/10.1021/es203355v, 2012.

Fibiger, D. L. and Hastings, M. G.: First Measurements of the Nitrogen Isotopic Composition of NO_x from Biomass Burning, Environ. Sci. Technol., 50, 11569–11574, https://doi.org/10.1021/acs.est.6b03510, 2016.

Fountoukis, C. and Nenes, A.: ISORROPIA II: a computationally efficient thermodynamic equilibrium model for K^+–Ca^{2+}–Mg^{2+}–NH_4^+–Na^+–SO_4^{2-}–NO_3^-–Cl^-–H_2O aerosols, Atmos. Chem. Phys., 7, 4639–4659, https://doi.org/10.5194/acp-7-4639-2007, 2007.

Freyer, H. D.: Seasonal variation of 15N / 14N ratios in atmospheric nitrate species, Tellus B, 43, 30–44, https://doi.org/10.1034/j.1600-0889.1991.00003.x, 1991.

Freyer, H. D., Kley, D., Volz-Thomas, A., and Kobel, K.: On the interaction of isotopic exchange processes with photochemical reactions in atmospheric oxides of nitrogen, J. Geophys. Res., 98, 14791, https://doi.org/10.1029/93JD00874, 1993.

Goldberg, D. L., Saide, P. E., Lamsal, L. N., de Foy, B., Lu, Z., Woo, J.-H., Kim, Y., Kim, J., Gao, M., Carmichael, G., and Streets, D. G.: A top-down assessment using OMI NO_2 suggests an underestimate in the NO_x emissions inventory in Seoul, South Korea, during KORUS-AQ, Atmos. Chem. Phys., 19, 1801–1818, https://doi.org/10.5194/acp-19-1801-2019, 2019.

Guha, T., Lin, C. T., Bhattacharya, S. K., Mahajan, A. S., Ou-Yang, C.-F., Lan, Y.-P., Hsu, S. C., and Liang, M.-C.: Isotopic ratios of nitrate in aerosol samples from Mt. Lulin, a high-altitude station in Central Taiwan, Atmos. Environ., 154, 53–69, https://doi.org/10.1016/J.ATMOSENV.2017.01.036, 2017.

Hallquist, M., Stewart, D. J., Stephenson, S. K., and Anthony Cox, R.: Hydrolysis of N_2O_5 on sub-micron sulfate aerosols, Phys. Chem. Chem. Phys., 5, 3453, https://doi.org/10.1039/b301827j, 2003.

He, P., Xie, Z., Chi, X., Yu, X., Fan, S., Kang, H., Liu, C., and Zhan, H.: Atmospheric $\Delta^{17}O(NO_3^-)$ reveals nocturnal chemistry dominates nitrate production in Beijing haze, Atmos. Chem. Phys., 18, 14465–14476, https://doi.org/10.5194/acp-18-14465-2018, 2018.

He, P., Xie, Z., Yu, X., Wang, L., Kang, H., and Yue, F.: The observation of isotopic compositions of atmospheric nitrate in Shanghai China and its implication for reactive nitrogen chemistry, Sci. Total Environ., 714, 136727, https://doi.org/10.1016/J.SCITOTENV.2020.136727, 2020.

Heaton, T. H. E.: $^{15}N/^{14}N$ ratios of NO_x from vehicle engines and coal-fired power stations, Tellus B, 42, 304–307, https://doi.org/10.1034/j.1600-0889.1990.00007.x-i1, 1990.

Ishino, S., Hattori, S., Savarino, J., Jourdain, B., Preunkert, S., Legrand, M., Caillon, N., Barbero, A., Kuribayashi, K., and Yoshida, N.: Seasonal variations of triple oxygen isotopic compositions of atmospheric sulfate, nitrate, and ozone at Dumont d'Urville, coastal Antarctica, Atmos. Chem. Phys., 17, 3713–3727, https://doi.org/10.5194/acp-17-3713-2017, 2017.

Kaiser, J., Hastings, M. G., Houlton, B. Z., Rockmann, T., and Sigman, D. M.: Triple oxygen isotope analysis of nitrate using the denitrifier method and thermal decomposition of N_2O, Anal. Chem., 79, 599–607, https://doi.org/10.1021/ac061022s, 2007.

Kamezaki, K., Hattori, S., Iwamoto, Y., Ishino, S., Furutani, H., Miki, Y., Uematsu, M., Miura, K., and Yoshida, N.: Tracing the sources and formation pathways of atmospheric particulate nitrate over the Pacific Ocean using stable isotopes, Atmos. Environ., 209, 152–166, https://doi.org/10.1016/J.ATMOSENV.2019.04.026, 2019.

Kang, H., Zhu, B., Gao, J., He, Y., Wang, H., Su, J., Pan, C., Zhu, T., and Yu, B.: Potential impacts of cold frontal passage on air quality over the Yangtze River Delta, China, Atmos. Chem. Phys., 19, 3673–3685, https://doi.org/10.5194/acp-19-3673-2019, 2019.

Kim, H., Zhang, Q., and Sun, Y.: Measurement report: Characterization of severe spring haze episodes and influences of long-range transport in the Seoul metropolitan area in March 2019, Atmos. Chem. Phys., 20, 11527–11550, https://doi.org/10.5194/acp-20-11527-2020, 2020.

Kim, H. C., Kim, S., Lee, S.-H., Kim, B.-U., and Lee, P.: Fine-Scale Columnar and Surface NO_x Concentrations over South Korea: Comparison of Surface Monitors, TROPOMI, CMAQ and CAPSS Inventory, Atmosphere-Basel, 11, 101, https://doi.org/10.3390/atmos11010101, 2020.

Kim, S.-W., Yoon, S.-C., Kim, J., and Kim, S.-Y.: Seasonal and monthly variations of columnar aerosol optical properties over east Asia determined from multi-year MODIS, LIDAR, and

AERONET Sun/sky radiometer measurements, Atmos. Environ., 41, 1634–1651, https://doi.org/10.1016/j.atmosenv.2006.10.044, 2007.

Lee, H.-J., Jo, H.-Y., Kim, S.-W., Park, M.-S., and Kim, C.-H.: Impacts of atmospheric vertical structures on transboundary aerosol transport from China to South Korea, Sci. Rep., 9, 13040, https://doi.org/10.1038/s41598-019-49691-z, 2019.

Lelieveld, J., Evans, J. S., Fnais, M., Giannadaki, D., and Pozzer, A.: The contribution of outdoor air pollution sources to premature mortality on a global scale, Nature, 525, 367–371, https://doi.org/10.1038/nature15371, 2015.

Li, D. and Wang, X.: Nitrogen isotopic signature of soil-released nitric oxide (NO) after fertilizer application, Atmos. Environ., 42, 4747–4754, https://doi.org/10.1016/j.atmosenv.2008.01.042, 2008.

Li, H., Zhang, Q., Zheng, B., Chen, C., Wu, N., Guo, H., Zhang, Y., Zheng, Y., Li, X., and He, K.: Nitrate-driven urban haze pollution during summertime over the North China Plain, Atmos. Chem. Phys., 18, 5293–5306, https://doi.org/10.5194/acp-18-5293-2018, 2018.

Li, J., Zhang, X., Orlando, J., Tyndall, G., and Michalski, G.: Quantifying the nitrogen isotope effects during photochemical equilibrium between NO and NO_2: implications for $\Delta^{15}N$ in tropospheric reactive nitrogen, Atmos. Chem. Phys., 20, 9805–9819, https://doi.org/10.5194/acp-20-9805-2020, 2020.

Li, J., Davy, P., Harvey, M., Katzman, T., Mitchell, T., and Michalski, G.: Nitrogen isotopes in nitrate aerosols collected in the remote marine boundary layer: Implications for nitrogen isotopic fractionations among atmospheric reactive nitrogen species, Atmos. Environ., 245, 118028, https://doi.org/10.1016/j.atmosenv.2020.118028, 2021.

Li, Z., Walters, W. W., Hastings, M. G., Zhang, Y., Song, L., Liu, D., Zhang, W., Pan, Y., Fu, P., and Fang, Y.: Nitrate Isotopic Composition in Precipitation at a Chinese Megacity: Seasonal Variations, Atmospheric Processes, and Implications for Sources, Earth Sp. Sci., 6, 2200–2213, https://doi.org/10.1029/2019EA000759, 2019.

Lim, S., Lee, M., Czimczik, C. I., Joo, T., Holden, S., Mouteva, G., Santos, G. M., Xu, X., Walker, J., Kim, S., Kim, H. S., Kim, S., and Lee, S.: Source signatures from combined isotopic analyses of $PM_{2.5}$ carbonaceous and nitrogen aerosols at the peri-urban Taehwa Research Forest, South Korea in summer and fall, Sci. Total Environ., 655, 1505–1514, https://doi.org/10.1016/j.scitotenv.2018.11.157, 2019.

Lim, S., Yang, X., Lee, M., Li, G., Gao, Y., Shang, X., Zhang, K., Czimczik, C. I., Xu, X., Bae, M.-S., Moon, K.-J., and Jeon, K.: Fossil-driven secondary inorganic $PM_{2.5}$ enhancement in the North China Plain: Evidence from carbon and nitrogen isotopes, Environ. Pollut., 266, 115163, https://doi.org/10.1016/J.ENVPOL.2020.115163, 2020.

Liu, Z., Gao, W., Yu, Y., Hu, B., Xin, J., Sun, Y., Wang, L., Wang, G., Bi, X., Zhang, G., Xu, H., Cong, Z., He, J., Xu, J., and Wang, Y.: Characteristics of $PM_{2.5}$ mass concentrations and chemical species in urban and background areas of China: emerging results from the CARE-China network, Atmos. Chem. Phys., 18, 8849–8871, https://doi.org/10.5194/acp-18-8849-2018, 2018.

McIlvin, M. R. and Casciotti, K. L.: Technical updates to the bacterial method for nitrate isotopic analyses, Anal. Chem., 83, 1850–1856, https://doi.org/10.1021/AC1028984, 2011.

Michalski, G. and Bhattacharya, S. K.: The role of symmetry in the mass independent isotope effect in ozone, P. Natl. Acad. Sci. USA, 106, 5493–5496, https://doi.org/10.1073/PNAS.0812755106, 2009.

Michalski, G., Scott, Z., Kabiling, M., and Thiemens, M. H.: First measurements and modeling of $\Delta^{17}O$ in atmospheric nitrate, Geophys. Res. Lett., 30, 1870, https://doi.org/10.1029/2003GL017015, 2003.

Michalski, G., Meixner, T., Fenn, M., Hernandez, L., Sirulnik, A., Edith Allen, A., and Thiemens, M.: Tracing Atmospheric Nitrate Deposition in a Complex Semiarid Ecosystem Using $\Delta^{17}O$, Environ. Sci. Technol., 38, 2175–2181, https://doi.org/10.1021/ES034980+, 2004.

Morin, S., Savarino, J., Frey, M. M., Domine, F., Jacobi, H.-W., Kaleschke, L., and Martins, J. M. F.: Comprehensive isotopic composition of atmospheric nitrate in the Atlantic Ocean boundary layer from 65° S to 79° N, J. Geophys. Res., 114, D05303, https://doi.org/10.1029/2008JD010696, 2009.

Morin, S., Sander, R., and Savarino, J.: Simulation of the diurnal variations of the oxygen isotope anomaly ($\Delta^{17}O$) of reactive atmospheric species, Atmos. Chem. Phys., 11, 3653–3671, https://doi.org/10.5194/acp-11-3653-2011, 2011.

Nelson, D. M., Tsunogai, U., Ding, D., Ohyama, T., Komatsu, D. D., Nakagawa, F., Noguchi, I., and Yamaguchi, T.: Triple oxygen isotopes indicate urbanization affects sources of nitrate in wet and dry atmospheric deposition, Atmos. Chem. Phys., 18, 6381–6392, https://doi.org/10.5194/acp-18-6381-2018, 2018.

Park, Y., Park, K., Kim, H., Yu, S., Noh, S., Kim, M., Kim, J., Ahn, J., Lee, M., Seok, K., and Kim, Y.: Characterizing isotopic compositions of TC−C, NO_3^-−N, and NH_4^+−N in $PM_{2.5}$ in South Korea: Impact of China's winter heating, Environ. Pollut., 233, 735–744, https://doi.org/10.1016/J.ENVPOL.2017.10.072, 2018.

Parnell, A. C., Inger, R., Bearhop, S., and Jackson, A. L.: Source Partitioning Using Stable Isotopes: Coping with Too Much Variation, PLoS One, 5, e9672, https://doi.org/10.1371/journal.pone.0009672, 2010.

Parnell, A. C., Phillips, D. L., Bearhop, S., Semmens, B. X., Ward, E. J., Moore, J. W., Jackson, A. L., Grey, J., Kelly, D. J., and Inger, R.: Bayesian stable isotope mixing models, Environmetrics, 24, 387–399, https://doi.org/10.1002/env.2221, 2013.

Quan, J., Dou, Y., Zhao, X., Liu, Q., Sun, Z., Pan, Y., Jia, X., Cheng, Z., Ma, P., Su, J., Xin, J., and Liu, Y.: Regional atmospheric pollutant transport mechanisms over the North China Plain driven by topography and planetary boundary layer processes, Atmos. Environ., 221, 117098, https://doi.org/10.1016/J.ATMOSENV.2019.117098, 2020.

Rose, L. A., Yu, Z., Bain, D. J., and Elliott, E. M.: High resolution, extreme isotopic variability of precipitation nitrate, Atmos. Environ., 207, 63–74, https://doi.org/10.1016/J.ATMOSENV.2019.03.012, 2019.

Saunders, S. M., Jenkin, M. E., Derwent, R. G., and Pilling, M. J.: Protocol for the development of the Master Chemical Mechanism, MCM v3 (Part A): tropospheric degradation of non-aromatic volatile organic compounds, Atmos. Chem. Phys., 3, 161–180, https://doi.org/10.5194/acp-3-161-2003, 2003.

Savarino, J., Kaiser, J., Morin, S., Sigman, D. M., and Thiemens, M. H.: Nitrogen and oxygen isotopic constraints on the origin of

atmospheric nitrate in coastal Antarctica, Atmos. Chem. Phys., 7, 1925–1945, https://doi.org/10.5194/acp-7-1925-2007, 2007.

Savarino, J., Morin, S., Erbland, J., Grannec, F., Patey, M. D., Vicars, W., Alexander, B., and Achterberg, E. P.: Isotopic composition of atmospheric nitrate in a tropical marine boundary layer., P. Natl. Acad. Sci. USA, 110, 17668–73, https://doi.org/10.1073/pnas.1216639110, 2013.

Shao, P., Tian, H., Sun, Y., Liu, H., Wu, B., Liu, S., Liu, X., Wu, Y., Liang, W., Wang, Y., Gao, J., Xue, Y., Bai, X., Liu, W., Lin, S., and Hu, G.: Characterizing remarkable changes of severe haze events and chemical compositions in multi-size airborne particles (PM_1, $PM_{2.5}$ and PM_{10}) from January 2013 to 2016–2017 winter in Beijing, China, Atmos. Environ., 189, 133–144, https://doi.org/10.1016/J.ATMOSENV.2018.06.038, 2018.

Sharma, H. D., Jervis, R. E., and Wong, K. Y.: Isotopic exchange reactions in nitrogen oxides, J. Phys. Chem., 74, 923–933, https://doi.org/10.1021/j100699a044, 1970.

Shi, C., Nduka, I. C., Yang, Y., Huang, Y., Yao, R., Zhang, H., He, B., Xie, C., Wang, Z., and Yim, S. H. L.: Characteristics and meteorological mechanisms of transboundary air pollution in a persistent heavy $PM_{2.5}$ pollution episode in Central-East China, Atmos. Environ., 223, 117239, https://doi.org/10.1016/J.ATMOSENV.2019.117239, 2020.

Song, W., Wang, Y.-L., Yang, W., Sun, X.-C., Tong, Y.-D., Wang, X.-M., Liu, C.-Q., Bai, Z.-P., and Liu, X.-Y.: Isotopic evaluation on relative contributions of major NO_x sources to nitrate of $PM_{2.5}$ in Beijing, Environ. Pollut., 248, 183–190, https://doi.org/10.1016/J.ENVPOL.2019.01.081, 2019.

Song, W., Liu, X.-Y., Wang, Y.-L., Tong, Y.-D., Bai, Z.-P., and Liu, C.-Q.: Nitrogen isotope differences between atmospheric nitrate and corresponding nitrogen oxides: A new constraint using oxygen isotopes, Sci. Total Environ., 701, 134515, https://doi.org/10.1016/J.SCITOTENV.2019.134515, 2020.

Stein, A. F., Draxler, R. R., Rolph, G. D., Stunder, B. J. B., Cohen, M. D., and Ngan, F.: NOAA's HYSPLIT Atmospheric Transport and Dispersion Modeling System, B. Am. Meteorol. Soc., 96, 2059–2077, https://doi.org/10.1175/BAMS-D-14-00110.1, 2015.

Thiemens, M. H.: Mass-Independent Isotope Effects in Planetary Atmospheres and the Early Solar System, Science, 283, 341–345, https://doi.org/10.1126/science.283.5400.341, 1999.

Thiemens, M. H.: HISTORY AND APPLICATIONS OF MASS-INDEPENDENT ISOTOPE EFFECTS, Annu. Rev. Earth Planet. Sci., 34, 217–262, https://doi.org/10.1146/annurev.earth.34.031405.125026, 2006.

Tong, D., Zhang, Q., Liu, F., Geng, G., Zheng, Y., Xue, T., Hong, C., Wu, R., Qin, Y., Zhao, H., Yan, L., and He, K.: Current Emissions and Future Mitigation Pathways of Coal-Fired Power Plants in China from 2010 to 2030, Environ. Sci. Technol., 52, 12905–12914, https://doi.org/10.1021/acs.est.8b02919, 2018.

van der Werf, G. R., Randerson, J. T., Giglio, L., Collatz, G. J., Mu, M., Kasibhatla, P. S., Morton, D. C., DeFries, R. S., Jin, Y., and van Leeuwen, T. T.: Global fire emissions and the contribution of deforestation, savanna, forest, agricultural, and peat fires (1997–2009), Atmos. Chem. Phys., 10, 11707–11735, https://doi.org/10.5194/acp-10-11707-2010, 2010.

Vicars, W. C. and Savarino, J.: Quantitative constraints on the ^{17}O-excess (Δ^{17}O) signature of surface ozone: Ambient measurements from 50° N to 50° S using the nitrite-coated filter technique, Geochim. Cosmochim. Acta, 135, 270–287, https://doi.org/10.1016/J.GCA.2014.03.023, 2014.

Vicars, W. C., Bhattacharya, S. K., Erbland, J., and Savarino, J.: Measurement of the ^{17}O-excess (Δ^{17}O) of tropospheric ozone using a nitrite-coated filter, Rapid Commun. Mass Spectrom., 26, 1219–1231, https://doi.org/10.1002/rcm.6218, 2012.

Wahner, A., Mentel, T. F., Sohn, M., and Stier, J.: Heterogeneous reaction of N_2O_5 on sodium nitrate aerosol, J. Geophys. Res. Atmos., 103, 31103–31112, https://doi.org/10.1029/1998JD100022, 1998.

Walters, W. W. and Michalski, G.: Theoretical calculation of nitrogen isotope equilibrium exchange fractionation factors for various NO_y molecules, Geochim. Cosmochim. Acta, 164, 284–297, https://doi.org/10.1016/J.GCA.2015.05.029, 2015.

Walters, W. W. and Michalski, G.: Theoretical calculation of oxygen equilibrium isotope fractionation factors involving various NO molecules, OH, and H_2O and its implications for isotope variations in atmospheric nitrate, Geochim. Cosmochim. Acta, 191, 89–101, https://doi.org/10.1016/j.gca.2016.06.039, 2016.

Walters, W. W., Goodwin, S. R., and Michalski, G.: Nitrogen Stable Isotope Composition (δ^{15}N) of Vehicle-Emitted NO_x, Environ. Sci. Technol., 49, 2278–2285, https://doi.org/10.1021/es505580v, 2015.

Walters, W. W., Simonini, D. S., and Michalski, G.: Nitrogen isotope exchange between NO and NO_2 and its implications for δ^{15}N variations in tropospheric NO_x and atmospheric nitrate, Geophys. Res. Lett., 43, 440–448, https://doi.org/10.1002/2015GL066438, 2016.

Walters, W. W., Fang, H., and Michalski, G.: Summertime diurnal variations in the isotopic composition of atmospheric nitrogen dioxide at a small midwestern United States city, Atmos. Environ., 179, 1–11, https://doi.org/10.1016/J.ATMOSENV.2018.01.047, 2018.

Wang, Y., Wang, Y., Wang, L., Petäjä, T., Zha, Q., Gong, C., Li, S., Pan, Y., Hu, B., Xin, J., and Kulmala, M.: Increased inorganic aerosol fraction contributes to air pollution and haze in China, Atmos. Chem. Phys., 19, 5881–5888, https://doi.org/10.5194/acp-19-5881-2019, 2019a.

Wang, Y., Song, W., Yang, W., Sun, X., Tong, Y., Wang, X., Liu, C., Bai, Z., and Liu, X.: Influences of Atmospheric Pollution on the Contributions of Major Oxidation Pathways to PM $_{2.5}$ Nitrate Formation in Beijing, J. Geophys. Res. Atmos., 124, 4174–4185, https://doi.org/10.1029/2019JD030284, 2019b.

Xie, Y., Dai, H., Zhang, Y., Wu, Y., Hanaoka, T., and Masui, T.: Comparison of health and economic impacts of $PM_{2.5}$ and ozone pollution in China, Environ. Int., 130, 104881, https://doi.org/10.1016/J.ENVINT.2019.05.075, 2019.

Xu, W., Sun, Y., Wang, Q., Zhao, J., Wang, J., Ge, X., Xie, C., Zhou, W., Du, W., Li, J., Fu, P., Wang, Z., Worsnop, D. R., and Coe, H.: Changes in Aerosol Chemistry From 2014 to 2016 in Winter in Beijing: Insights From High-Resolution Aerosol Mass Spectrometry, J. Geophys. Res. Atmos., 124, 1132–1147, https://doi.org/10.1029/2018JD029245, 2019.

Yu, Z. and Elliott, E. M.: Novel method for nitrogen isotopic analysis of soil-emitted nitric oxide, Environ. Sci. Technol., 51, 6268–6278, https://doi.org/10.1021/acs.est.7b00592, 2017.

Zhao, H., Zhang, X., Zhang, S., Chen, W., Tong, D., Xiu, A., Zhao, H., Zhang, X., Zhang, S., Chen, W., Tong, D. Q., and Xiu, A.: Effects of Agricultural Biomass Burning on Re-

gional Haze in China: A Review, Atmosphere-Basel, 8, 88, https://doi.org/10.3390/atmos8050088, 2017.

Zheng, H., Kong, S., Wu, F., Cheng, Y., Niu, Z., Zheng, S., Yang, G., Yao, L., Yan, Q., Wu, J., Zheng, M., Chen, N., Xu, K., Yan, Y., Liu, D., Zhao, D., Zhao, T., Bai, Y., Li, S., and Qi, S.: Intra-regional transport of black carbon between the south edge of the North China Plain and central China during winter haze episodes, Atmos. Chem. Phys., 19, 4499–4516, https://doi.org/10.5194/acp-19-4499-2019, 2019.

Zong, Z., Wang, X., Tian, C., Chen, Y., Fang, Y., Zhang, F., Li, C., Sun, J., Li, J., and Zhang, G.: First assessment of NO_x sources at a regional background site in north China using isotopic analysis linked with modeling, Environ. Sci. Technol., 51, 5923–5931, https://doi.org/10.1021/acs.est.6b06316, 2017.

Zong, Z., Tan, Y., Wang, X., Tian, C., Li, J., Fang, Y., Chen, Y., Cui, S., and Zhang, G.: Dual-modelling-based source apportionment of NO_x in five Chinese megacities: Providing the isotopic footprint from 2013 to 2014, Environ. Int., 137, 105592, https://doi.org/10.1016/J.ENVINT.2020.105592, 2020.